Tetraaryl Pyrenes: Photophysical Properties, Computational Studies, Crystal Structures, and Application in OLEDs

Tarek H. El-Assaad,[1] Manuel Auer,[2] Raul Castañeda,[3] Kassem H. Hallal,[1] Fadi M. Jradi,[1] Lorenzo Mosca,[4] Rony S. Khnayzer,[5] Digambara Patra,[1] Tatiana V. Timofeeva,[3] Jean-Luc Brédas,[6] Emil J. W. List-Kratochvil,[2,7] Brigitte Wex,[5,*] and Bilal R. Kaafarani[1,*]

[1]*Department of Chemistry, American University of Beirut, Beirut 1107-2020, Lebanon*
[2]*NanoTecCenter Weiz Forschungsgesellschaft mbH, Franz-Pichler-Straße 32, A-8160 Weiz, Austria*
[3]*Department of Biology & Chemistry, New Mexico Highlands University, Las Vegas, NM 87701, USA*
[4]*Department of Chemistry and Center for Photochemical Sciences, Bowling Green State University, Bowling Green, Ohio, 43403, USA*
[5]*Department of Natural Sciences, Lebanese American University, Byblos, Lebanon*
[6]*Solar & Photovoltaics Engineering Research Center, Physical Science and Engineering Division, King Abdullah University of Science & Technology, Thuwal 23955-6900, Kingdom of Saudi Arabia*
[7]*Institute of Solid State Physics, Graz University of Technology, A-8010 Graz, Austria*

[*] To whom correspondence should be addressed. Email: brigitte.wex@lau.edu.lb (B.W.) ; bilal.kaafarani@aub.edu.lb (B.R.K.)

Abstract

Pyrene was derivatized in positions 1, 3, 6, and 8 to yield a series of nine tetraarylpyrenes for which absorption, emission and emission lifetimes and solvatochromism in solution were determined. The fluorescence quantum yields in thin film and crystalline state, electrochemistry, and quantum-chemical calculations were completed for the series along with X-ray crystal structure analysis of compounds **1**, **2**, **4**, **5**, **7**, and **9**. Compounds **2**, **3**, **4** as well as **7** were identified as most suitable candidates for OLED application. Notably, in an unoptimized single-layer device geometry, these compounds exhibited blue electroluminescence coupled to impressively low turn-on voltages and high maximum luminances such as 2.8 V and 13,542 cd m-^{2} at 8.2 V for compound **2**, respectively.

Keywords: tetraarylpyrenes, photophysical studies, solid state fluorescence, OLED

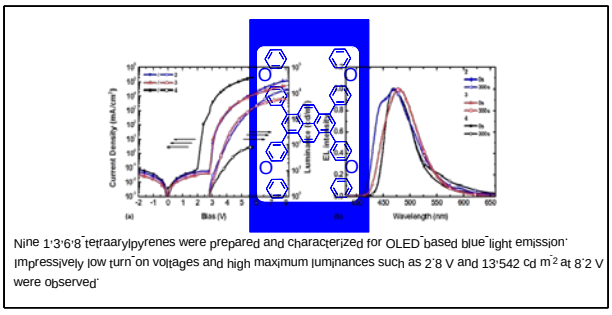

Introduction

Pyrene, the polycyclic aromatic hydrocarbon, has made a broad impact on a wide range of scientific fields such as analytical[1,2] and bioorganic chemistry[3] as well as organic electronics, as reported by Figueira-Duarte and Müllen[4] in their seminal review. Therein, the significance of the pyrene core, particularly as a material combining high chemical stability, charge-carrier mobility and blue-light emission was highlighted for use in organic light-emitting diodes (OLEDs).[4] The fluorescent nature of pyrene[5,6,7] and of the pyrene excimer[5,8-10] has been widely investigated both in the solid state and in solution. The pyrene excimer is an interaction between a ground state and an excited state molecule when in close proximity and is characterized by a marked bathochromic shift in the maximum emission wavelength.[7] To overcome excimer formation, steric functionalization of the pyrene core is necessary.[11] Synthetic strategies for substitution at various positions were thoroughly reviewed[4,12] and a wealth of pyrene derivatives have been studied for emissive properties and application in optoelectronic devices such as, monosubstituted,[13,14] 1,3-disubstituted pyrenes[15] 1,6-disubstituted pyrenes,[16] 1,8-disubstituted pyrenes,[17] and 2,7-disubstituted pyrenes.[18-20] Y-shaped, 1,3,7-trisubstituted pyrene derivatives exhibit blue emission with medium to high fluorescence quantum yield ranging from 0.38 to 0.78 in solution and 0.42 to 0.69 in thin film.[21] Among tetraarylpyrenes, 1,3,5,9-tetrasubstitutedpyrenes,[22] 4,5,9,10-tetrasubstitutedpyrenes,[23,24] and 1,3,6,8-tetrasubstitutedpyrenes[25,26,27] were studied. The inclusion of tri- and tetrasubstituted phenyl derivatives onto the pyrene backbone yields amorphous materials with only modest photoluminescence quantum yields of 0.28-0.38 in solution (0.24-0.44 in solid state),[25] which highlights the importance of substituent selection on photophysical properties. Particularly, 1,3,6,8-tetraphenylpyrene (TPP) has raised considerable interest as blue emitting material for organic light-emitting diodes (OLEDs),[25] and organic light-emitting field-effect transistors (OLEFETs)[28] applications. Derivatives of TPP with 7-*tert*-butylpyrene, 9,9-bis(3-methylbuty)-9H-fluoren-2-yl and 4-methoxyphenyl yield materials with high fluorescence quantum yields of 0.75-0.99 in dichloromethane solution.[26] Compound 1,3,6,8-tetrakis[4-2,2-diphenylvinyl)phenyl]pyrene was used as emitter in OLED application and shows a turn-on voltage of 3.51 V, a max. luminance of 103,835 cdm^{-2} with a max. current efficiency of 5.19 cdA^{-1}.[29] However, there is a marked absence of a systematic study of the substitution pattern. Herein, we report the study of structure-property relationships of nine compounds; eight 1,3,6,8-tetraphenylpyrenes embellished with electron donating and electron withdrawing substituents

specifically on the four phenyl rings and of one 1,3,6,8-tetrathiophen-2-ylpyrene. We further report the X-ray crystal structures of six compounds (**1**, **2**, **4**, **5**, **7**, **9**) and importantly explore device characteristics in OLED geometries for compounds **2**, **3**, **4**, and **7**.

Materials and Methods

1,3,6,8-tetrabromopyrene,[30] tetrakis(triphenylphosphine)palladium(0)[31] were synthesized according to literature procedures.

Compounds **1**, **3**, **6**, and **7** were synthesized according to a common literature procedure.[27] To 30 mL of toluene were added 1,3,6,8-tetrabromopyrene (0.50 g, 0.97 mmol) and the corresponding boronic acid (5.82 mmol) followed by 3 mL of 2M aqueous K_2CO_3, and catalytic amount of tetrabutylammonium bromide. The mixture was purged with Argon for 20 min, before tetrakis(triphenylphosphine)palladium(0) (67 mg, 0.057 mmol) was added and the mixture was stirred at 110 ^oC for 48 hrs or 72 hrs for compounds **1** and **3** or **6** and **7**, respectively. After evaporation of the solvent under reduced pressure, the obtained solid was triturated with chloroform using Soxhlet extraction apparatus. The chloroform extract was then washed with 5% K_2CO_3 aqueous solution (2 x 50 mL) followed by brine (2 x 50 mL). The organic phase was dried over $MgSO_4$, filtered, and solvent removed under reduced pressure. Note, due to insolubility, compound **6** was directly obtained by filtration at this stage.

1,3,6,8-tetrakis(4-(tert-butyl)phenyl)pyrene (1)

The obtained beige solid was then purified by column chromatography starting with hexanes as the mobile phase, and then increasing the polarity to 5% dichloromethane in hexanes to obtain the desired product, which was then recrystallized from toluene first, then from chloroform to yield **1** (0.50 g, 70%) as a shiny white solid. ^1H NMR (500 MHz, $CDCl_3$): δ 8.14 (s, 4H), 7.97 (s, 2H), 7.55 (d, J = 8.5 Hz, 8H), 7.49 (d, J = 8.5 Hz, 8H), 1.35 (s, 36H). ^{13}C NMR (125 MHz, $CDCl_3$): δ 150.1, 138.1, 136.9, 130.3, 129.5, 129.0, 128.0, 126.0, 125.2, 34.6, 31.4. Anal. Calcd. For $C_{56}H_{58}$: C, 92.00; H, 8.00. Found: C, 91.97; H, 8.06. T_d = 439.1 ^oC.

1,3,6,8-tetrakis(3,4,5-trimethoxyphenyl)pyrene (3)

The obtained orange solid was recrystallized from toluene to yield **3** (0.40 g, 48%) as yellow crystals. ^{1}H NMR (500 MHz, $CDCl_3$): δ 8.18 (s, 4H), 7.97 (s, 2H), 6.80 (s, 8H), 3.90 (s, 12H), 3.84 (s, 24H). ^{13}C NMR (125 MHz, $CDCl_3$): δ 153.1, 137.4, 137.2, 136.4, 128.9, 128.1, 125.8, 125.3, 107.8, 61.0, 56.25. Anal. Calcd. For $C_{52}H_{50}O_{12}$: C, 72.04; H, 5.81. Found: C, 71.85; H, 5.84. T_d = 408.7 ^{o}C

1,3,6,8-tetrakis(3,5-difluorophenyl)pyrene (6)

The obtained dark green, insoluble solid was recrystallized from 1,2-dichlorobenzene to yield **6** (0.25 g, 40%) as shiny yellow greenish needle-like crystals. No NMR data could be collected due to insolubility. Anal. Calcd. For $C_{40}H_{18}F_8$: C, 73.85; H, 2.79. Found: C, 73.67; H, 2.69. T_d = 368.2 ^{o}C.

1,3,6,8-tetrakis(3,5-bis(trifluoromethyl)phenyl)pyrene (7)

The obtained solid was recrystallized from chlorobenzene to yield **7** (0.68 g, 67%) as shiny white solid. ^{1}H NMR (500 MHz, $CDCl_3$): δ 8.05 (s, 8H), 8.03 (s, 4H), 7.99 (s, 4H), 7.95 (s, 2H), ^{13}C NMR (125 MHz, $CDCl_3$): δ 141.5, 135.1, 132.9, 132.4, 132.0, 131.5, 130.55, 129.5, 128.8, 125.8, 125.5, 125.0, 121.9, 121.4 Anal. Calcd. For $C_{48}H_{18}F_{24}$: C, 54.87; H, 1.73. Found: C, 54.90; H, 1.61. T_d = 318.4 ^{o}C.

Compounds **2**[32], **4**[32], **5**[33] were synthesized according to a common literature procedure[34]

1,3,6,8-tetrabromopyrene (0.50 g, 0.97 mmol) was added to 20 mL isopropanol, then the corresponding boronic acid (4.39 mmol) was added. The mixture was purged with Argon for 20 min, after which palladium (II) acetate (0.70 mg, 3.12 μmol), triphenylphosphine (2.47 mg, 9.42 μmol), and 0.56 mL of 2M aqueous K_2CO_3 solution were added, followed by 0.34 mL of deionized water. The mixture was refluxed for 36 hrs under Argon atmosphere and in the dark. The reaction was cooled to room temperature, quenched with water and extracted with ethyl acetate The

combined organic layer was washed with a 5% aqueous K_2CO_3 solution and with a brine solution, and solvent was removed under reduced pressure.

1,3,6,8-tetrakis(4-phenoxyphenyl)pyrene (2)

The obtained yellow needle-like crystals were purified by column chromatography starting with hexanes as a mobile phase, then increasing the polarity to 5% dichloromethane in hexanes to obtain **2** (0.42 g, 49%) as a white solid. ^{1}H NMR (500 MHz, $CDCl_3$): δ 8.14 (s, 4H), 7.94 (s, 2H), 7.57 (d, J = 8.5 Hz, 8H), 7.34 (t, J = 8.0 Hz, 8H), 7.12 (d, J = 8.5 Hz, 8H), 7.08-7.06 (m, 12H). ^{13}C NMR (125 MHz, $CDCl_3$): δ 157.1, 156.8, 136.6, 135.9, 131.9, 129.8, 129.0, 128.1, 126.0, 125.2, 123.5, 119.1, 118.6. Anal. Calcd. For $C_{64}H_{42}O_4$: C, 87.85; H, 4.84. Found: C, 87.91; H, 4.96. T_d = 503.6 ^{o}C.

1,3,6,8-tetrakis(4-(methylthio)phenyl)pyrene (4)[32]

The obtained solid was recrystallized from toluene to yield **4** as a yellow solid (1.00 g, 29%). ^{1}H NMR (500 MHz, $CDCl_3$): δ 8.09 (s, 4H), 7.89 (s, 2H), 7.53 (d, J = 8.0 Hz, 8H), 7.37 (d, J = 8.0 Hz, 8H), 2.52 (s, 12H). ^{13}C NMR (125 MHz, $CDCl_3$): δ 137.7, 136.6, 131.0, 129.4, 129.05, 128.1, 126.4, 126.0, 125.2, 15.85. Anal. Calcd. For $C_{44}H_{34}S_4$: C, 76.48; H, 4.96; S, 18.56. Found: C, 76.60; H, 5.09; S, 18.41. T_d = 392.4 ^{o}C.

1,3,6,8-tetrakis(4-fluorophenyl)pyrene (5)[33]

The obtained greenish solid was recrystallized from toluene to yield **5** (0.70 g, 24%) as yellow crystals. ^{1}H NMR (500 MHz, $CDCl_3$): δ 8.05 (s, 4H), 7.87 (s, 2H), 7.56 (dd, $^3J_{H-H}$ = 8.5 Hz, $^3J_{H-F}$ = 5.5 Hz, 8H), 7.17 (d, J = 8.5 Hz, 8H). ^{13}C NMR (125 MHz, $CDCl_3$): δ 163.4 (d, $^1J_{C-F}$ = 245 Hz), 136.7 (d, $^4J_{C-F}$ = 2.5 Hz), 136.3, 132.1 (d, $^3J_{C-F}$ = 7.5 Hz), 129.6, 128.2, 125.8, 125.3, 115.5 (d, $^2J_{C-F}$ = 20 Hz). Anal. Calcd. For $C_{40}H_{22}F_4$: C, 83.03; H, 3.83. Found: C, 82.92; H, 4.01. T_d = 381.8 ^{o}C.

Compounds **8**[35] and **9**[36] were synthesized according to a literature procedure.[30]

Tetramethyl 4,4',4'',4'''-(pyrene-1,3,6,8-tetrayl)tetrabenzoate (8)[35]

Yellow solid **8** (3.00 g, 73%). ^{1}H NMR (500 MHz, $CDCl_3$): δ 8.15 (d, J = 8.0 Hz, 8H), 8.07 (s, 4H), 7.92 (s, 2H), 7.67 (d, J = 8.0 Hz, 8H), 3.91 (s, 12H). ^{13}C NMR (125 MHz, $CDCl_3$): δ 166.9, 145.35, 136.5, 130.6, 129.7, 129.2, 129.2, 128.3, 125.7, 125.5, 52.3. Anal. Calcd. For $C_{48}H_{34}O_8$: C, 78.04; H, 4.64. Found: C, 78.31; H, 4.77.

1,3,6,8-tetrakis(thiophen-2-yl)pyrene (9)[36]

Light orange solid **9** (0.78 g, 17%). ^{1}H NMR (500 MHz, $CDCl_3$): δ 8.45 (s, 4H), 8.17 (s, 2H), 7.46 (dd, J = 5.0, 1.0 Hz, 4H), 7.34 (dd, J = 3.5, 1.0 Hz, 4H), 7.20 (dd, J = 5.0, 3.5 Hz, 4H). ^{13}C NMR (125 MHz, $CDCl_3$): δ 141.8, 131.2, 129.7, 129.1, 128.35, 127.5, 126.5, 125.8, 125.7. Anal. Calcd. For $C_{32}H_{18}S_4$: C, 72.42; H, 3.42; S, 24.17. Found: C, 72.33; H, 3.28; S, 24.06. T_d = 400.1 ^{o}C.

Electrochemical Analysis

Electrochemical measurements were carried out under an inert atmosphere in dry deoxygenated dichloromethane (DCM) solution containing 0.1 M tetrabutylammonium hexafluorophosphate as electrolyte. A CH-Instrument 620D potentiostat equipped with a conventional three-electrode cell utilizing a glassy carbon working electrode, platinum wire counter electrode, and a silver wire coated with silver chloride as the pseudo-reference electrode, was used for the measurements. Potentials were referenced to decamethylferrocene/decamethyferrocenium ($DMFc/DMFc^+$) couple by using decamethylferrocene as an internal standard. All measured potentials were converted to ferrocene/ferrocenium scale; ($DMFc/DMFc^+$) was measured to be -0.54 vs. Fc/Fc^+ in DCM.

Computational details

Ground-state molecular geometries and vibrational frequencies of isolated compounds **1**-**9** were determined at the Density Functional Theory (DFT) level, with the B3LYP functional and the 6-31G(d,p) basis set. Vertical first electronic singlet excited states were explored at the time-dependent (TD) DFT and Tamm-Dancoff approximation (TDA) levels using both the B3LYP functional and the range-separated hybrid functional ωB97[37] with the 6-31G(d,p) basis set. For the ωB97 functional, the ω value for each compound was tuned with respect to the ionization potential (IP-tuning) by minimizing J(ω) in Eq. 1 where $\epsilon^{\omega}_{HOMO}(N)$ is the HOMO energy of the neutral

molecule (with N electrons) and $E_{gs}(\omega, N)$ and $E_{gs}(\omega, N-1)$ represents the total energy of the neutral molecule and the cation, respectively:[38]

$$J(\omega) = |\epsilon^{\omega}_{HOMO} - (E_{gs}(\omega, N) - E_{gs}(\omega, N-1)| \quad (1)$$

The following omega (ω) values were obtained: 0.148 (**1**); 0.143 (**2**); 0.145 (**3**); 0.149 (**4**); 0.162 (**5**); 0.162 (**6**); 0.155 (**7**); 0.150 (**8**); 0.165 (**9**); 0.162 (TPP); 0.248 (pyrene). The Polarizable Continuum Model (PCM) in its integral equation formalism variant (IEFPCM) was used at the TDDFT level to explore the first singlet electronic excited states of **1**-**9**, TPP and pyrene in tetrahydrofuran. All calculations were carried out with the Gaussian09 (Revision D.01) software.[39]

Photophysical studies

Solution

The absorption and fluorescence excitation and emission spectra were acquired for **1**-**9** using 100 μM (for UV-visible measurements) and 1-2 μM (for fluorescence measurements) of each compound prepared in different solvents. For UV-visible spectral measurements a JASCO V-570 UV-NIR spectrophotometer was used, whereas fluorescence measurements were done using a Jobin-Yvon-Horiba Fluorolog III spectrofluorimeter. The excitation source was a 100 W xenon lamp and the slit width was fixed at 5 nm for all measurements. The fluorescence lifetime was measured using the same instrument. The fluorescence quantum yields (Φ_f) were evaluated according to the following equation 2:

$$\Phi_{unk} = \Phi_{std} \frac{F_{unk}}{F_{std}} \frac{A_{std}}{A_{unk}} \frac{n^2_{unk}}{n^2_{std}} \qquad \textbf{Equation 2}$$

where standard (std) refers to the reference sample (i.e. 9,10-diphenyl anthracence in cyclohexane) and unkown (unk) refers to compounds (**1**-**9**), wherein, the quantum yield of 9,10-diphenyl anthracence in cyclohexane was taken as 1.0. *F* corresponds to the integrated intensity of the

emission spectra of the sample or reference, while *A* is the optical density of the sample or reference at the excitation wavelength. Finally, *n* is the refractive index of the solvent being used.[40]

Solid state

Absolute fluorescence quantum yields in crystalline solids and thin films were acquired on a Hamamatsu Quantaurus-QY (C11347) instrument equipped with a CCD multichannel detector, a spectralon integrating sphere and xenon lamp excitation.

X-ray crystal structure analysis

X-ray diffraction experiments were carried out with a Bruker SMART APEX II CCD diffractometer, using Mo Kα radiation (λ = 0.71073 Å) at 100 K for compounds **1**, **2**, **5**, **7** and **9,** and at 297 K for compound **4**, while no suitable crystals were obtained for the remaining materials. The raw data frames were integrated with the SAINT+ program using narrow-frame algorithm.[41] Absorption corrections were applied using the semi-empirical method of the SADABS program.[42] The structures were solved by direct methods and refined using Olex2[43] by full-matrix least-squares methods on F^2 with SHELXL-97 in anisotropic approximation for all non-hydrogen atoms. The main crystallographic data are summarized in Table 7. CIF files of compounds **1**, **2**, **4**, **5**, **7**, and **9** have been deposited and allocated the following CCDC deposition numbers 1044326, 1015953, 1011328, 1011330, 1015949 and 1039264, respectively.

Organic light-emitting devices and characterization

Electroluminescence characteristics of the new compounds were investigated in devices featuring them as the active layer in a standard sandwich geometry: indium tin oxide (ITO)/poly(3,4-ethylenedioxythiophene)-poly-styrenesulfonic acid (Baytron P VPAI 4083) (PEDOT:PSS)/**2**, **3**, **4** and **7**/Ca/Al. ITO-covered glass substrates were first carefully rinsed with deionized water, acetone and isopropyl alcohol. Afterwards the substrates were subjected to various ultrasonic treatments in detergent, deionized water, acetone, and isopropanol. A dry cleaning step in oxygen plasma finished the cleaning procedure while at the same time providing an enhancement of the surface wettability of PEDOT:PSS. Consecutively, a layer of PEDOT:PSS was applied via spin-coating under ambient conditions and dried under ambient conditions at 200 °C for 5 minutes. The active layers were evaporated at a rate of 0.6 Å s^{-1} from a resistively heated crucible under dynamic vacuum at an initial base pressure lower than 1.0×10^{-6} mbar. The layer thicknesses were controlled

by a quartz-crystal microbalance and verified by a Veeco Dimension V atomic force microscope equipped with a Nanoscope V controller in tapping mode at several positions. The resulting layer thickness amounted to 80 nm. The cathode materials (Ca, Al) were deposited onto the substrate with thicknesses of 10 nm and 100 nm for Ca and Al respectively without breaking the vacuum through a shadow mask. Consequently multiple devices with a device-area of 10 mm^2 were formed on a single substrate. Electroluminescence (EL) spectra were acquired using an ORIEL spectrometer with an attached calibrated charge-coupled device (CCD) camera. Current–luminance–voltage (I–L–V) characteristics were recorded in a customized setup using a Keithley 2612A source measure unit for recording the I–V characteristics while the luminance was measured by a Keithley 6517 Electrometer using a photodiode calibrated by a Konica-Minolta LS-100 Luminancemeter.

Results and Discussion

Synthesis

Electrophilic aromatic substitution of the commercially available pyrene in the presence of nitrobenzene afforded 1,3,6,8-tetrabromopyrene (**Py-Br$_4$**) in 98% yield.[37] Suzuki coupling of **Py-Br$_4$**[30] with a series of electron-rich, and electron-poor phenyl boronic acids yielded (*p*-*t*-butyl **1**, *p*-phenoxy **2**, 3',4',5'-trimethoxy **3** and methylthio **4**[32]), and (*p*-fluoro **5**[33], 3,5-difluoro **6**, 3,5-trifluoromethyl **7**, methoxycarbonyl **8**[44]), respectively. In addition, the reaction of **Py-Br$_4$** with 2-thiophene boronic acid yielded 1,3,6,8-tetrathienylpyrene **9**, Scheme 1. Compounds **2**, **3**, and **6** are new compounds, while compounds **1** and **7** have been previously been reported only in patents leaving experimental data inaccessible. Several Suzuki-Miyaura cross-coupling procedures with a variety of solvents such as toluene,[27] isopropanol[34] or 1,4-dioxane (dioxane[30]) were tested. The procedure invoking toluene was found to be most suitable in the synthesis of **1**, **3**, **6**, and **7**. Isopropanol was found to be the solvent of choice for the synthesis of compounds **2**, **4** and **5**, while dioxane was found to be the preferred solvent for the preparation of **8** and **9**.

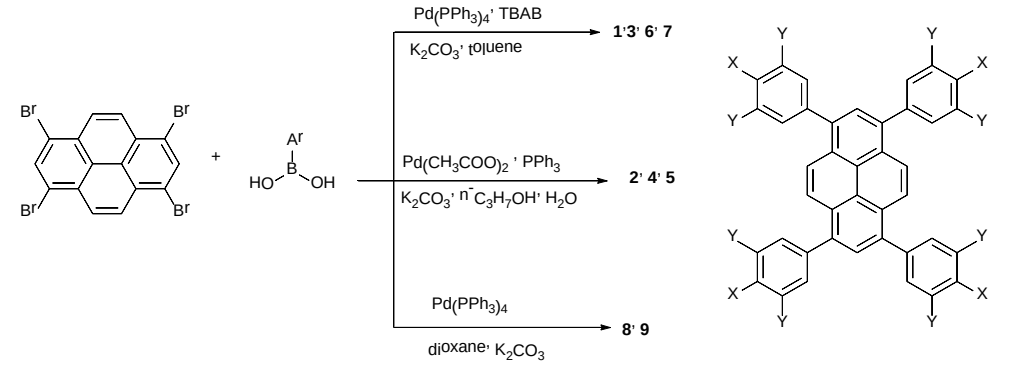

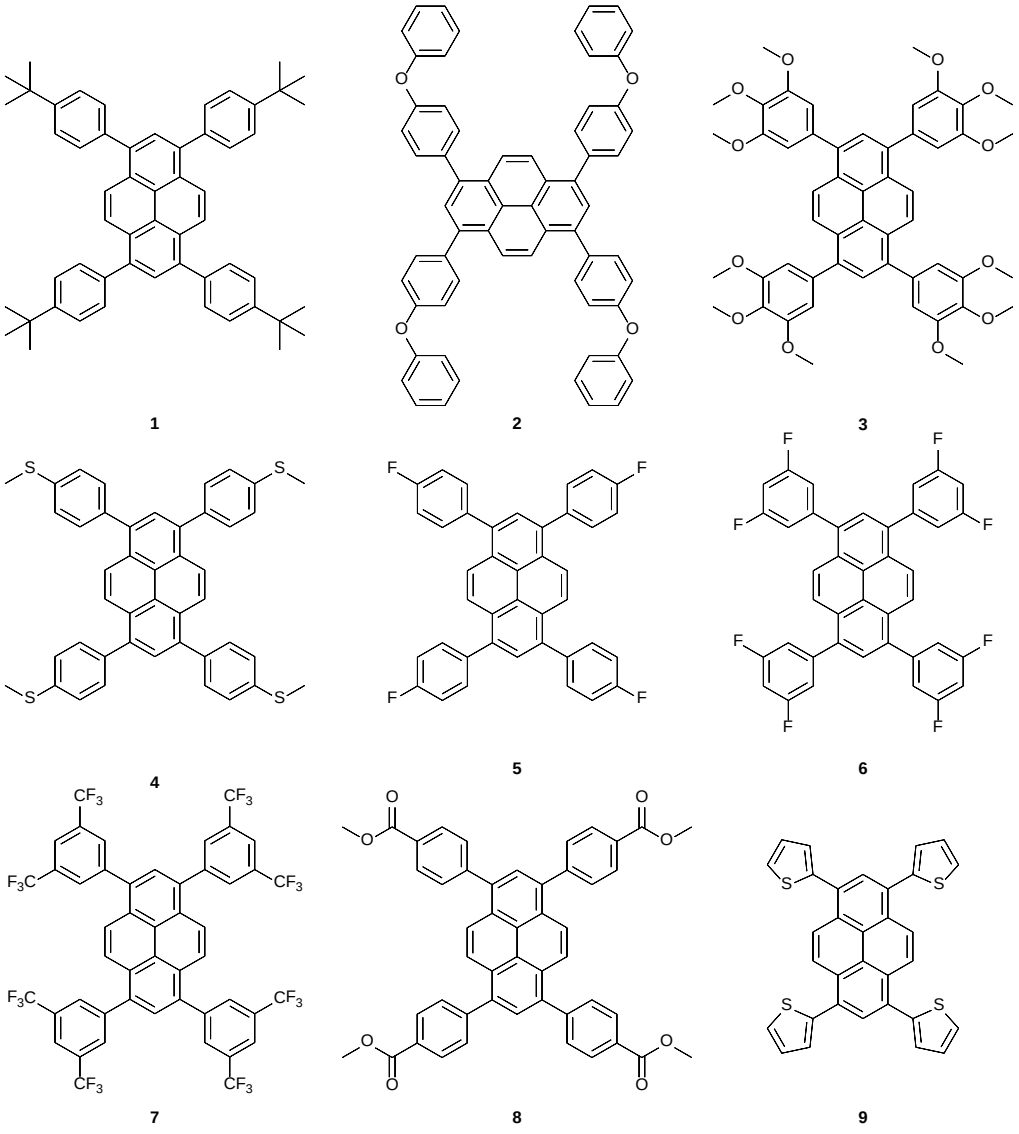

Scheme 1. Synthetic approach of target compounds **1**-**9**.

Photophysical Studies

Pyrene is a well-characterized chromophore with four absorption bands as observed in a cyclohexane solution; a low energy electronic transition $S_0 \rightarrow S_1$ at 372 nm (ε = 510 $mol^{-1}cm^{-1}L$) with vibrational fine structure, followed by higher energy electronic $S_0 \rightarrow S_2$, $S_0 \rightarrow S_3$ and $S_0 \rightarrow S_4$ transitions at 334 (ε = 55,000 $mol^{-1}cm^{-1}L$), 272 (ε = 54,000 $mol^{-1}cm^{-1}L$), and 243 nm (ε = 88,000 $mol^{-1}cm^{-1}L$), respectively.[19] According to Platt nomenclature, the two lowest-lying $\pi \rightarrow \pi^*$ transitions lead to excited states L_a and L_b. L_a is due to a HOMO-LUMO excitation polarized along the long axis of pyrene, while L_b is due to degenerate HOMO-1→LUMO and HOMO→LUMO+1 configurations polarized along the short axis of pyrene.[45] L_b is the lowest energy $S_0 \rightarrow S_1$ transition and is symmetry forbidden. A low fluorescence quantum yield for pyrene is thus observed. The second transition L_a, also referred to as $S_0 \rightarrow S_2$ energy transition, is symmetry allowed and characterized by large oscillator strength. A modulation of the fluorescence quantum yield hinges on lowering of the energy level of this transition compared to L_b. Substitution in positions 2,7 does not result in a change of the molecular orbital levels due to the presence of a nodal plane along these positions. A substitution on positions 1, 1 & 6, 1 & 8 and 4 & 9[46] in pyrene, however, modulates the allowed transition and thus results in materials with a large oscillator strength for the $S_0 \rightarrow S_1$ transition and high fluorescence quantum yields.[47] TPP, the pyrene derivative with phenyl substituents at the 1, 3, 6 and 8 positions shows a marginal loss of features in both absorption and fluorescence spectra coupled to a red shift in absorption (~350 nm) and fluorescence spectra (~420 nm).[48] TPP shows an increased fluorescence quantum yield of 0.84 compared to 0.29 for pyrene in aerated cyclohexane solution (0.90 compared to 0.60 in non-aerated cyclohexane solution).[49] The significant increase is additionally attributed to steric inhibition of excimer formation.[49] Interestingly, even though the intersystem crossing rate (k_{ST}) increased from 0.16 x 10^7 s^{-1} to 3.7 x 10^7 s^{-1}, the fluorescence rate constant (k_f) value increased from 0.25 x 10^7 s^{-1} to 33.3 x 10^7 s^{-1} when going from the planar pyrene molecule to the non-planar TPP.[49] Particularly in vacuum deposited thin film, TPP showed a high photoluminescence quantum efficiency of 68 ± 3%.[33] In the present case, we aim to deduce the effect on the photophysical properties of introducing electron donating and electron withdrawing substituents on the four phenyl rings of TPP.

The UV-visible absorption and fluorescence spectra of compounds **1-9** in chloroform are shown in Figure 1. All compounds showed two transitions: one in the region 350 - 440 nm for the $S_0 \rightarrow S_1$ absorption transition and the other in the region 250 -330 nm for the $S_0 \rightarrow S_n$ (n >1) absorption. When taking TPP as a reference, a bathochromic shift was observed in the UV-visible spectrum ($S_0 \rightarrow S_1$ transition) of **1-9**. The bathochromic shift of at least 25 nm or more depended on the nature of the substitution on the phenyl units. The overall largest shift was observed for tetrathienyl derivative **9**[50] followed by substituted TPP **4**, **8**, and **2** whereas **3**, **5**, **6** and **7** exhibited only marginal shifts. It should be noted that structural features in the absorption spectrum still appeared in **1**, **5, 6,** and **7** but could not be resolved for **3**, **4**, **8**, **9** and were poorly resolved in **2**.

In contrast, in the fluorescence spectra, **5** and **7** did not show any remarkable shift compared to parent TPP.[33] Nevertheless, the bathochromic shift in fluorescence spectra increased from **6**, **1**, **2**, **3**, **8**, **4**, and **9**. The structural features in the fluorescence spectra were also lost in **2**, **3**, **8**, and **9** and relatively resolved in **1**, **4**, **5**, **6**, and **7**. To make sure these structural features are not due to excimer formation as commonly observed in pyrene, we measured the emission spectra at different excitation wavelengths in 350 – 450 nm range in chloroform for all the compounds; no changes in position of the emission spectra were observed except for a variation in fluorescence intensity due to change in absorbance in these excitation wavelengths. This suggests there is only one emitting species in all the compounds. Similarly, when the excitation spectra were recorded at various possible emission wavelengths in the 390-540 nm range, no changes in the spectral positions in the excitation spectra were found which rules out any possible excimer formation in these compounds at the studied concentration. The representative absorption, excitation and emission fluorescence spectra for compound **5** (with structural feature in the spectrum) and **9** (without any structural feature in the spectrum) are summarized in Figure 2 (for other compounds, see ESI). The excitation spectra for these compounds look similar to their respective absorption spectra, even the structural features could be seen in the excitation spectra for compounds **1**, **5**, and **7** similar to their absorption spectra. The fluorescence spectra were also found to be mirroring the absorption spectra. From these observations, it can be concluded that both the absorbing and emitting species are the same for all these compounds. Therefore, the absorption and fluorescence spectral changes among different compounds are due to a fine balance between conformational effects and electronic effects linked to the substitution of the phenyl units by electron-rich groups.[25]

From the shape of absorption and fluorescence spectra, such as relatively resolved structural features for **5, 6** and **7** and completely structureless features for **8** and **9**, it can be concluded that these compounds exhibit a noticeable conformational disorder associated to the rotation of the external rings. This interpretation is consistent with the earlier observation by Moorthy *et al*[25] who restricted the rotation of the external rings by substituting methyl groups at the two ortho-positions of phenyl group and found well-resolved absorption and fluorescence spectra in dichloromethane.[25] Stokes shifts ($\Delta\lambda$) along with absorption and emission maxima for compounds **1**-**9** in chloroform are summarized in Table 1. Compounds **8** and **9** have the largest Stokes shift whereas compounds **1**, **5**, **6** and **7** have the smallest (ESI). This reflects a trend similar to that found for the structural features of the compounds, thus, suggesting that rotation of the external rings plays a significant role in the spectral properties though restriction of rotation could be influenced by electronic effects. For instance, the electron-donating nature of substituents in **1** and the electron-withdrawing nature in **5, 6** and **7** might create a partial double bond character (extending the conjugation of the pyrene moiety into the phenyl group) thus restricting rotation. At the same time, the thienyl moiety in **9** could rotate easily around the single bond making the conjugation between pyrene moiety and thienyl group less effective. For the case of **8**, the conjugation between methylbenzoate group and pyrene moiety is limited since the conjugation would need to create two negative charges (on oxygen) in the opposite site (two negative charges) and thus would strain the system.

The fluorescence quantum yields for compounds **1-9** in chloroform are summarized in Table 1. Fluorescence quantum yield ranged from 75% to 98% for all compounds except **9** with only 17%. No obvious trend was observed. Thiophene rings decrease fluorescence quantum yield when linked to as opposed to fused onto a core,[51] thus leading to the relatively low fluorescence quantum yield for compound **9** compared to rest of the compounds. The fluorescence lifetime of these compounds was measured under argon atmosphere and the decay profile is shown in Figure 2. When the fluorescence lifetime was measured at various possible emission wavelengths keeping the excitation wavelength constant there was no change in fluorescence lifetime (see ESI), which further confirms absence of excimer. The fluorescence decay profile for all these compounds in chloroform could be fit to a single exponential decay (see ESI). The presence of a single

exponential decay further suggests that emission emanates from a single excited state. The rate constant for radiative decay (k_r) is calculated by the following equation:[40]

$$k_r = \frac{\Phi_f}{\tau_f}$$

while k_{nr}, i.e. the average non-radiative rate constant, was calculated by equation:[40]

$$\boldsymbol{k_{nr} = k_{tot} - k_r}$$

The fluorescence lifetimes, rate constant for radiative decay and average non-radiative rate constant for various compounds in chloroform are gathered in Table 2. The fluorescence lifetimes of these compounds were found to be in the 0.5 – 2.5 ns range in chloroform as well as in cyclohexane (discussed later on). It should be noted that a significant decrease in experimental fluorescence lifetime occurred upon moving from pyrene (405 ns) to TPP (3 ns).[49] The fluorescence lifetime further decreased in substituted TPP (< 3 ns) depending on the nature and position of the substituent. The highest lifetime values were attributed to the fluorine containing compounds and the lowest values were attributed to the sulfur containing compounds. The k_r values were found to be in the order of magnitude of TPP (3.33×10^8 s^{-1}) and k_{nr} values also did not show any trend except that k_{nr} value was highest for **9** (containing thiophene as substitution). This is also reflected in the comparably lower k_r, lifetime and most significantly in the low quantum yield value.

To investigate the solvatochromic behavior of these compounds, 8 different solvents namely: cyclohexane, 1,4-dioxane, tetrahydrofuran, chloroform, *N*,*N*-dimethylformamide, dimethylsulfoxide, acetonitrile and ethanol were selected. All the compounds showed variation in absorption and fluorescence spectra when changing solvent polarity. Compound **8** could not be measured in cyclohexane due to poor solubility. Figures 4 and 5 depict UV-visible absorption and fluorescence spectra of **5** and **9,** respectively. The structural features of both absorption and fluorescence spectra of **5** are retained upon changing the solvent environment. For all the compounds under investigation, it was observed that there is no change in spectral features by changing the solvent environment. However, for all compounds a positive solvatochomism was observed, whereby a red shift was detected in both absorption and fluorescence spectra while increasing the polarity of the solvent, which is as expected for a π- π^* transition. Sulfur-containing compounds **4** and **9** showed a clear red shift in all solvents in comparison with the other seven

compounds in both absorbance and emission spectra. The solvatochromic change of compounds **1-9** with respect to change in solvent environment could be better understood by evaluating the Stokes shift as given in Tables 2 and 3. The correlation of Stokes shift with solvent environment could be studied as per theory of general solvent effects and dielectric continuum theory.[40, 52] The plots of Stokes shift versus Δf (orientation polarizability) and E_T30 (solvent polarity scale) were generated for all compounds **1-9**. A common feature of compounds (**1-9**) is their minimal solvent effect as found by the near zero slope for plots of Stokes shifts versus Δf and E_T30 (see ESI). In few cases, the vibrationally structured fluorescence spectrum suggests a planar excited-state configuration as the origin of emission. Fused polycyclic aromatic compounds exhibit fluorescence spectra rich in vibronic structure, wherein a marked absence in solvatochromic effect is also well established.[18] The fluorescence lifetimes, quantum yields, radiative and non-radiative rate constants for compounds **1-9** are summarized in Tables 2 and 3. Unlike the UV-visible absorption and fluorescence spectra, these values did not show any systematic trend with solvent polarity. Indeed the estimated values for quantum yields and lifetimes were quite close in most cases and were within the error margin.

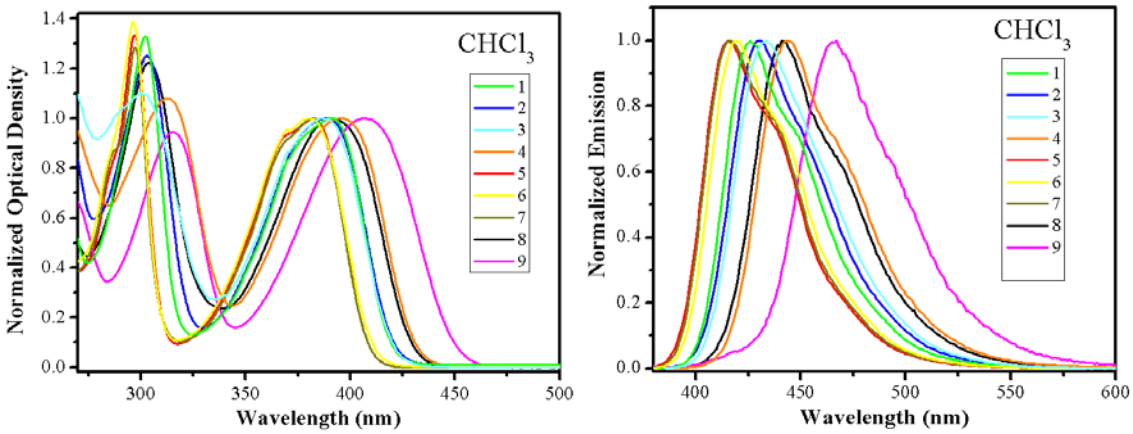

Figure 1. Normalized absorption (left) and normalized emission (right) spectra of compounds **1-9** in chloroform.

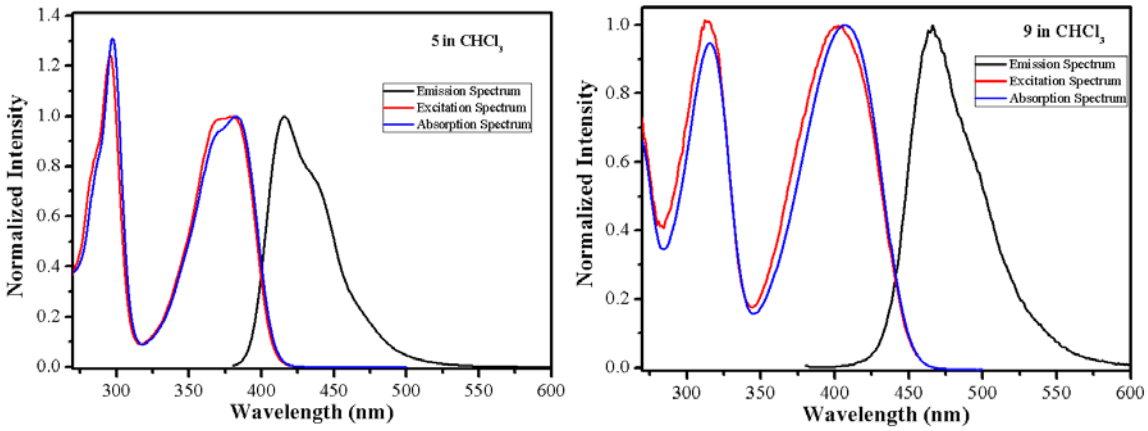

Figure 2. Normalized absorption, excitation and emission spectra of **5** (left) (λ_{ex}=370 nm; λ_{em}=440 nm) and **9** (right) in chloroform (λ_{ex}=370 nm; λ_{em}=466 nm).

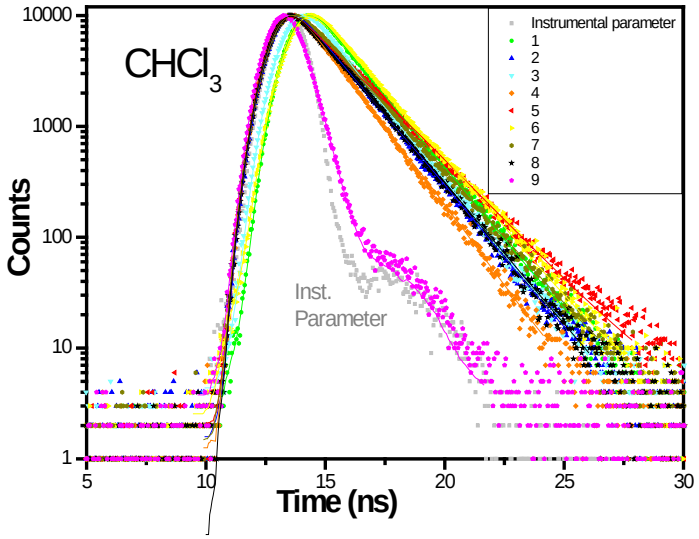

Figure 3. Time-resolved fluorescence decay profile for compounds **1**-**9** in chloroform.

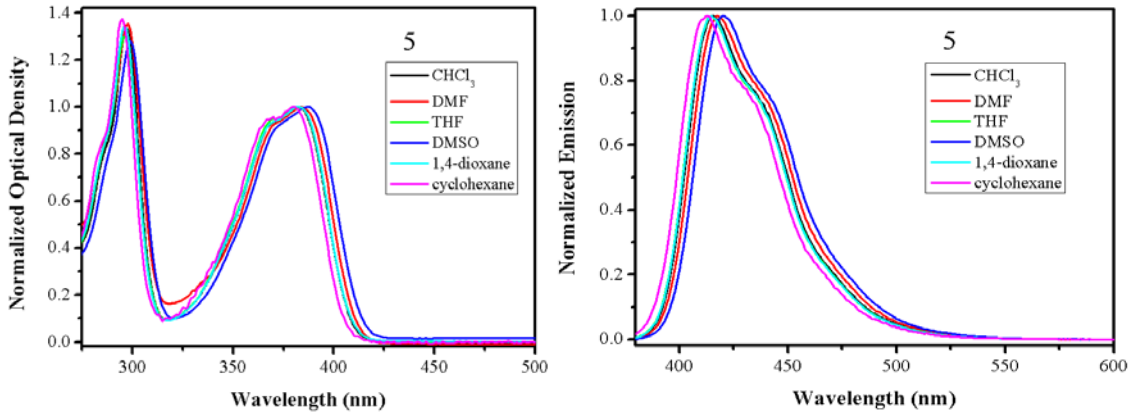

Figure 4. UV-visible absorption (left) and fluorescence (right) spectra of **5** in different solvent environments.

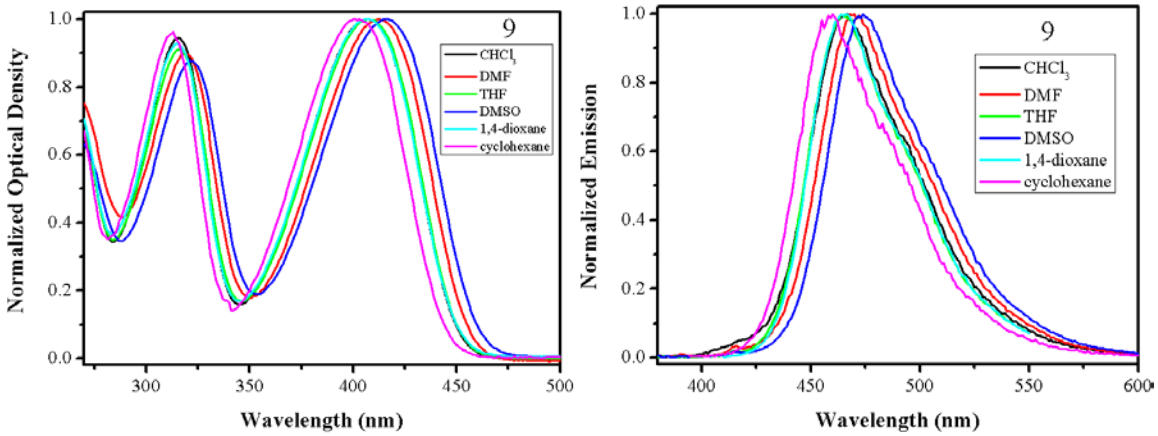

Figure 5. UV-visible absorption (left) and fluorescence (right) spectra of **9** in different solvent environments.

Table 1. Photophysical data in chloroform.

Compound	λ_{max}^{em} (in nm)	λ_{max}^{abs} (in nm)	$\Delta\lambda$ (in cm^{-1})	τ (in ns)	ϕ_F	k_r (in 10^8)s^{-1}	k_{nr} (in 10^8) s^{-1}
1	426	391	2101	1.83	0.97	5.30	0.16
2	430	388	2517	1.86	0.98	5.27	0.11
3	434	387	2798	1.75	0.85	4.86	0.86
4	444	396	2730	1.66	0.8	4.82	1.20
5	416	382	2140	2.27	0.84	3.70	0.70
6	419	380	2449	1.93	0.75	3.89	1.30
7	416	382	2140	2.02	0.88	4.36	0.59
8	443	391	3002	1.93	0.89	4.61	0.57
9	467	407	3157	0.54	0.17	3.15	15.40

Table 2. Photophysical data in various solvents. [⊥]

Compound	Solvent	λ_{max}^{em} (in nm)	λ_{max}^{abs} (in nm)	$\Delta\lambda$ (in cm^{-1})	τ (in ns)	ϕ_F	k_r (in 10^8) s^{-1}	k_{nr} (in 10^8) s^{-1}
1	chloroform	426	391	2101	1.83	0.97	5.30	0.16
1	DMF	428	393	2081	1.92	0.89	4.64	0.57
1	THF	424	390	2056	1.94	0.90	4.64	0.52
1	DMSO	--	--	--	--	--	--	--
1	1,4-dioxane	425	389	2178	1.89	0.82	4.34	0.95
1	cyclohexane	423	387	2199	1.89	0.81	4.29	1.01
2	chloroform	430	388	2517	1.86	0.98	5.27	0.11
2	DMF	432	391	2427	1.94	0.91	4.69	0.46
2	THF	429	389	2397	1.91	0.998	5.23	0.01
2	DMSO	434	387	2798	1.84	0.69	3.75	1.68
2	1,4-dioxane	429	389	2397	1.86	0.85	4.57	0.81
2	cyclohexane	425	384	2512	1.85	0.79	4.27	1.14
3	chloroform	434	387	2798	1.75	0.85	4.86	0.86
3	DMF	438	392	2679	1.99	0.83	4.17	0.85
3	THF	434	389	2665	1.88	0.75	3.99	1.33
3	DMSO	440	395	2589	1.95	0.78	4.00	1.13
3	1,4-dioxane	432	388	2625	1.83	0.75	4.10	1.37
3	cyclohexane	432	384	2894	1.75	0.93	5.31	0.40
4	chloroform	444	396	2730	1.66	0.80	4.82	1.20
4	DMF	447	400	2629	1.73	0.73	4.22	1.56
4	THF	442	396	2628	1.63	0.72	4.42	1.72
4	DMSO	450	403	2592	1.71	0.68	3.98	1.87
4	1,4-dioxane	441	396	2577	1.58	0.72	4.56	1.77
4	cyclohexane	437	396	2369	1.47	0.47	3.20	3.61
5	chloroform	416	382	2140	2.27	0.84	3.70	0.70
5	DMF	417	384	2061	2.34	0.87	3.72	0.56
5	THF	415	383	2013	2.51	0.81	3.23	0.76
5	DMSO	421	387	2087	2.13	0.84	3.94	0.75
5	1,4-dioxane	415	383	2013	2.44	0.82	3.36	0.74
5	cyclohexane	413	381	2034	2.74	0.83	3.03	0.62

[⊥] λ_{max}^{em} : Emission maximum ; λ_{max}^{abs} : Absorption maximum ; $\Delta\lambda$: Stokes shift; τ: Fluorescence lifetime; ϕ_F: Fluorescence quantum yield; k_r : radiative rate constant and k_{nr} : non-radiative rate constant.

Table 3. Photophysical data in various solvents.[⊥]

Compound	Solvent	λ_{max}^{em} (in nm)	λ_{max}^{abs} (in nm)	$\Delta\lambda$ (in cm^{-1})	τ (in ns)	ϕ_F	k_r (in 10^8) s^{-1}	k_{nr} (in 10^8) s^{-1}
6	chloroform	419	380	2449	1.93	0.75	3.89	1.30
6	DMF	425	381	2717	2.11	0.80	3.79	0.95
6	THF	422	383	2413	2.09	0.81	3.88	0.91
6	DMSO	427	386	2488	1.93	0.68	3.52	1.66
6	1,4-dioxane	419	382	2312	2.03	0.80	3.94	0.99
6	cyclohexane	415	379	2289	2.12	0.72	3.40	1.32
7	chloroform	416	382	2140	2.02	0.88	4.36	0.59
7	DMF	427	386	2488	2.13	0.91	4.27	0.42
7	THF	420	383	2300	2.14	0.85	3.97	0.70
7	DMSO	427	387	2421	2.07	--	--	--
7	1,4-dioxane	419	382	2312	2.08	0.80	3.85	0.96
7	cyclohexane	413	382	1965	2.18	0.93	4.27	0.32
8	chloroform	443	391	3002	1.93	0.89	4.61	0.57
8	DMF	446	393	3024	1.97	0.78	3.96	1.12
8	THF	440	390	2914	1.88	0.75	3.99	1.33
8	DMSO	448	398	2804	1.95	0.57	2.92	2.21
8	1,4-dioxane	441	390	2965	1.87	0.75	4.01	1.34
8	cyclohexane	--	--	--	1.78	--	--	--
9	chloroform	467	407	3157	0.54	0.17	3.15	15.4
9	DMF	470	413	2936	0.56	0.15	2.68	15.2
9	THF	464	408	2958	0.50	0.14	2.80	17.2
9	DMSO	474	416	2941	0.63	0.16	2.54	13.3
9	1,4-dioxane	466	407	3111	0.47	0.14	2.98	18.3
9	cyclohexane	460	403	3075	0.47	0.11	2.34	18.9

[⊥] λ_{max}^{em} : Emission maximum ; λ_{max}^{abs} : Absorption maximum ; $\Delta\lambda$: Stokes shift; τ: Fluorescence lifetime; ϕ_F: Fluorescence quantum yield; k_r : radiative rate constant and k_{nr} : non-radiative rate constant.

TDDFT with a B3LYP functional has to be used cautiously to model the lowest singlet excited states in large unsaturated molecules in general and for pyrene specifically since B3LYP tends to overdelocalize the wavefunctions.[45] Time-dependent DFT was used to compute the energies of the vertical transitions in the gas phase and in a solution environment. Table 4 shows results of TD-DFT and TDA calculations as an overview of vertical transition wavelengths and energies, oscillator strengths as well as transition dipole moments for pyrene, TPP and compounds **1**-**9** as calculated using B3LYP and ωB97 in the gas phase. As expected, all absorptions appear at shorter wavelength (higher energy) when going from B3LYP-TD to ωB97-TD to ωB97-TDA level of theory. In all cases, though, the general trends for compounds **1-9** are retained. For all compounds **1-9**, as for the TPP case, the $S_o \rightarrow S_1$ lowest energy transition is allowed with a high oscillator strength. This is in stark contrast to the situation of pyrene, where the lowest allowed transition is

of $S_o \rightarrow S_2$ nature.[5, 7] The calculated absorption maxima agree well with experimental data. For all compounds **1**-**9**, the lowest energy $S_o \rightarrow S_1$ transition is best described as HOMO→LUMO excitation with more than 95% contribution. When TDA-DFT was applied, the lowest energy transition presents a slight shift to higher energy as well as an increase in oscillator strength. The molecular orbitals involved in the $S_o \rightarrow S_1$ transition of **1**-**9** are shown in ESI. The lowest energy HOMO→LUMO transition broadly mimics the π-π* transition as observed in TPPs. For compound **1**, a small bathochromic shift in the vertical transition wavelength is observed attributed to the electron-donating nature of the alkyl groups. For compound **2** and **3** (**4**) an n-π* transitions involving O (S) are observed, which increases the effective conjugation resulting in bathochromic shifts in the vertical absorption with a largest effect of sulfur. However, the peripheral phenyl units in compound **2** are isolated from the chromophore. Interestingly, F is involved in n-π* transition only for compound **5**, i.e. p-fluorophenyl, yet not in compound **6**, i.e. 3,5-difluorophenyl substituent or compound **7**, i.e. 3,5-bis(trifluoromethyl)phenyl. In all three cases, the absorption maximum remains unaltered in comparison to TPP. For compounds **1**, **5**, **6**, and **7** a minor contribution of the HOMO-1→LUMO+1 transition of approx. 2% is observed similar to TPP, diminished in comparison to the 10% this transition contributes in pyrene. A delocalization of electron density toward the ester functionality is observed for compound **8** and into the thienyl units for compound **9**. The ground state to first excited state absorptions that include state-specific correction in THF solution are listed along with experimental data as acquired in THF. The computed values match well with the experimental data within few nm in general. For compounds **2**, **7**, and **8**, a 0.1 - 0.2 eV shift is observed between theory and experiment, Table 4.

Table 4. Time-dependent DFT and TDA results for wavelengths (λ_{vert}, nm), energies (E_{vert}, eV), oscillator strengths, and transition dipole moments (μ_{ge}, Debye) for the lowest transitions in compounds **1**-**9** in the gas phase.

Functional		B3LYP-TD				wB97-TD							Experiment	wB97-TDA			
Compound		λ_{vert} (nm)	E_{vert} (eV)	f	μ_{ge} (Debeye)	λ_{vert} (nm)	E_{vert} (eV)	f	μ_{ge} (Debeye)	Electronic configuration	λ_{vert} (nm) THF	E_{vert} (eV) THF	λ_{max} (nm) THF	λ_{vert} (nm)	E_{vert} (eV)	f	μ_{ge} (Debeye)
Pyrene	$S_o \rightarrow S_1$	333	3.72	0.256	2.814	315	3.94	0.000	0.000	HOMO-1→LUMO (47%) HOMO→LUMO+1 (50%)	307	4.04		310	4.00	0.000	0.000
	$S_o \rightarrow S_2$	328	3.78	0.000	0.000	309	4.02	0.321	3.258	HOMO-1→LUMO+1 (10%) HOMO→LUMO (90%)	315	3.94		292	4.25	0.360	3.460
TPP	$S_o \rightarrow S_1$	398	3.11	0.745	9.766	385	3.22	0.770	9.772	HOMO-1→LUMO+1 (3%) HOMO→LUMO (96%)	384	3.23		364	3.40	0.932	11.186
	$S_o \rightarrow S_2$	354	3.51	0.000	0.002	349	3.55	0.000	0.003	HOMO-→LUMO (39%) HOMO→LUMO+1 (53%)	353	3.51		350	3.54	0.000	0.001
1	$S_o \rightarrow S_1$	404	3.07	0.880	11.714	396	3.13	0.891	11.617	HOMO-1→LUMO+1 (2%) HOMO→LUMO (96%)	395	3.14	390	374	3.31	1.044	12.853
	$S_o \rightarrow S_2$	355	3.49	0.000	0.003	353	3.51	0.000	0.000					355	3.49	0.000	0.000
2	$S_o \rightarrow S_1$	413	3.00	0.977	13.282	404	3.05	1.004	13.355	HOMO→LUMO (95%)	404	3.07	389	382	3.25	1.185	14.890
	$S_o \rightarrow S_2$	361	3.43	0.025	0.292	358	3.47	0.002	0.022					358	3.46	0.002	0.021
3	$S_o \rightarrow S_1$	406	3.06	0.862	11.512	398	3.11	0.876	11.483	HOMO→LUMO (96%)	399	3.11	389	377	3.29	1.028	12.740
	$S_o \rightarrow S_2$	356	3.48	0.001	0.010	355	3.49	0.000	0.000					357	3.47	0.000	0.001
4	$S_o \rightarrow S_1$	424	2.93	0.910	12.694	406	3.05	0.966	12.928	HOMO→LUMO (95%)	405	3.06	396	385	3.22	1.157	14.662
	$S_o \rightarrow S_2$	371	3.34	0.114	1.399	358	3.46	0.006	0.068					359	3.45	0.005	0.058
5	$S_o \rightarrow S_1$	400	3.10	0.758	9.998	387	3.20	0.787	10.023	HOMO-1→LUMO+1 (2%) HOMO→LUMO (96%)	386	3.21	383	366	3.38	0.956	11.532
	$S_o \rightarrow S_2$	356	3.49	0.001	0.008	350	3.54	0.000	0.000					351	3.53	0.000	0.001
6	$S_o \rightarrow S_1$	400	3.10	0.740	9.733	386	3.21	0.766	9.739	HOMO-1→LUMO+1 (3%) HOMO→LUMO (96%)	384	3.23	383	365	3.40	0.925	11.105
	$S_o \rightarrow S_2$	354	3.50	0.001	0.006	349	3.55	0.000	0.003					350	3.54	0.000	0.002
7	$S_o \rightarrow S_1$	398	3.12	0.759	9.950	387	3.20	0.783	9.986	HOMO-1→LUMO+1 (2%) HOMO→LUMO (96%)	403	3.07	383	366	3.39	0.926	11.140
	$S_o \rightarrow S_2$	353	3.51	0.002	0.028	350	3.55	0.000	0.004					351	3.53	0.000	0.003
8	$S_o \rightarrow S_1$	418	3	0.870	11.988	402	3.08	0.922	12.198	HOMO→LUMO (100%)	420	2.95	390	397	3.12	1.159	15.154
	$S_o \rightarrow S_2$	362	3.43	0.025	0.294	354	3.50	0.001	0.006					365	3.40	0.000	0.002
9	$S_o \rightarrow S_1$	434	2.86	0.743	10.611	414	3.00	0.790	10.763	HOMO→LUMO (100%)	408	3.04	408	386	3.21	0.967	12.282
	$S_o \rightarrow S_2$	373	3.33	0.010	0.126	360	3.44	0.002	0.022					358	3.46	0.002	0.024

Emission in the solid state

Photophysical quantum yield data in the solid state were also collected. The emission spectra of compounds **1**-**9** obtained in the crystalline state and thin film were acquired, Figures 6 and 7. In general, we observed a bathochromic shift going from solution to crystalline solid-state emission by as low as 0.1 eV in the case of **1** and as high as 0.5 eV in the case of **9**. In addition, a bathochromic shift was also observed in the spin-coated thin film's emission versus the solution. It is noteworthy that the emission in the crystalline state vs. thin-film for **9** is exceptionally different, with a λ_{max} around 585 nm for the crystalline powder and 540 nm for thin-film. In the case of **9**, this might be due to aggregate emission in the crystalline state, which is suppressed or substantially modified in the thin-film. The absolute fluorescence quantum yield in the crystalline state ranged from 0.048 in compound **9** to 0.918 in compound **7**, Table 5. This trend was mirrored in the thin film with 0.077 for **9** and 0.911 for **7**. With the exception of **1**, **6**, and **8**, the compounds are more emissive in the thin film than in the crystalline state. Noteworthy is compound **3**, which shows merely 12% quantum yield in the crystalline form yet 88% in the thin film. This dramatic variation is attributed to the different packing of molecules in the crystal vs. the thin film. In most

cases, an increased intermolecular interaction is observed going from solution to thin-films and finally to crystalline solid. In general, thin-films show a lower crystallinity than a precipitated material, especially when the evaporation of the solvent is forced rapidly by spin-coating. The amorphous phases in the thin film are more susceptible to encapsulate residual solvent molecules and are therefore loosely packed. This might account for the increase in quantum yield of compounds **2**, **3**, **4**, **5** and **9** in thin-films vs. crystalline state. However, **1**, **6**, and **8** display the opposite trend and might signify an increase in packing density in the thin-film or it might be due to more complicated deactivation pathways. Our findings infer that the photophysical properties of these compounds are sensitive to the level of packing in the solid-state and are consistent with previous reports of a red-shift in the emission spectra of pyrene derivatives due to different types of packing[53, 54] as different packings lead to different polarization energies, variations in ionization potential and electron affinities and hence transition energies.[55] In general, For TPP, annealed thin films and crystalline solids exhibit different photoluminescence properties while attaining the same crystal form.[56] In addition, different packing modes of 1-acetyl-3-(4-methoxyphenyl)-5-(1-pyrenyl)-pyrazoline (AMPP) that resulted from various crystallization strategies yielded different optical properties of the same compound.[53]

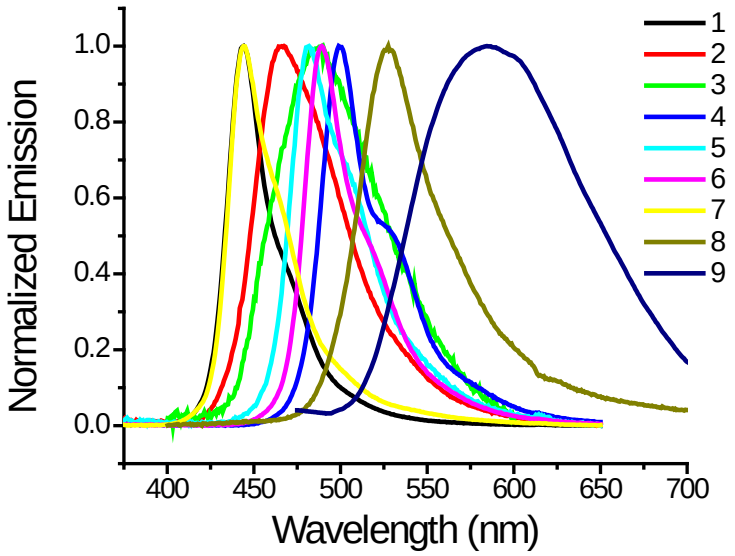

Figure 6. Fluorescence spectra of crystalline samples **1-9** at λ_{ex} = 320 nm.

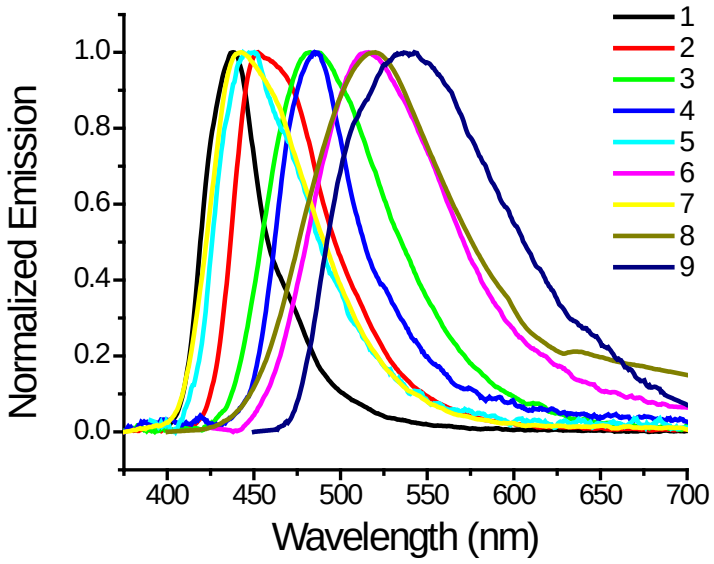

Figure 7. Fluorescence spectra of **1-9** in thin films at λ_{ex} = 320 nm.

Table 5. Absolute fluorescence quantum yield of compounds **1-9** in crystalline state (CR) and thin film (TF) λ_{ex} = 320 nm.

Compound	Φ_{CR}	Φ_{TF}
1	0.735	0.540
2	0.539	0.747
3	0.124	0.881
4	0.464	0.506
5	0.183	0.306
6	0.776	0.485
7	0.918	0.911
8	0.626	0.222
9	0.048	0.077

CR = crystalline state; TF=thin film prepared on glass substrates from solutions of 5 x 10^{-4} M in dichloromethane. The average error on the measurements above was 0.004.

Electrochemistry

The ionization potential (IP) of pyrene vs. vacuum was determined to be 5.6 eV (0.84 V vs Fc/Fc^{+} in DCM). [57] Solution electrochemistry experiments showed that the oxidation potential of pyrene is 1.3 eV vs SCE[58] and an effective blocking of reactive 1,3,6,8-positions in pyrene is necessary

to observe a clear, one electron, quasi-reversible oxidation to yield a relatively stable cation radical such as in TPP.[59] The oxidation potential of TPP was reported as 1.13 eV vs. SCE.[58] Functionalizing the TPP with electron donating groups on the dangling phenyl groups such as in compounds **1-5** or a 1,3,6,8-tetrathienyl-substituted pyrene **9** shifts the oxidation waves to a less positive potential, and hence decreases their IPs vs. vacuum, Figure 8 and Table 6, a behavior that was observed before.[57] On the other hand, adding electron withdrawing groups at the aforementioned phenyl rings in **7** and **8** shifts the oxidation potential in the opposite direction, increasing the IPs vs. vacuum by 0.10 and 0.30 eV, respectively. Due to insolubility of **6**, no data was acquired.

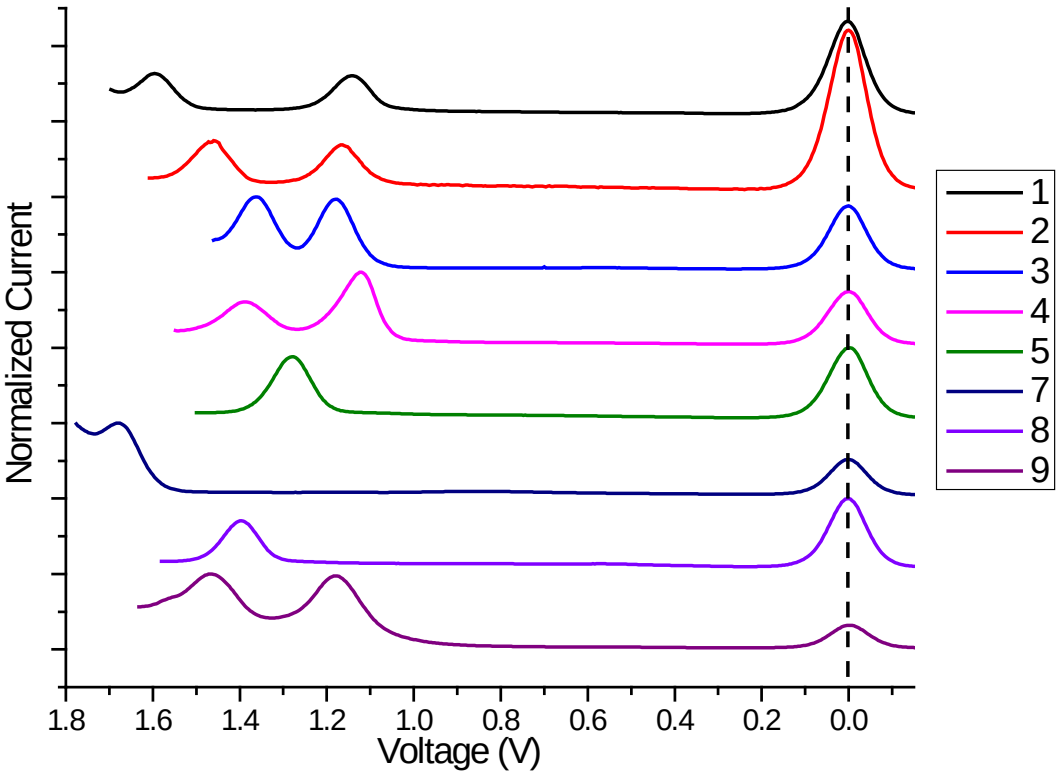

Figure 8. Differential pulse voltammetry (DPV) on the series **1**–**5** and 7–**9** in dichloromethane. Decamethyl-ferrocene (right) was used as an internal standard.

Table 6. Electrochemical potential and electrochemically estimated solid-state ionization potentials.

	$E_{1/2}^{+/0}$ [V][a]	$E_{1/2}^{2+/+}$ [V][a]	$E_{1/2}^{+/0}$ [V][b]	$E_{1/2}^{2+/+}$ [V][b]	IP(s) [eV][c]	λ_{onset} [nm]	E_g^{opt} [eV][f]	EA(s) [eV][f]
1	1.14	1.7	0.6	1.16	5.4	419	2.96	2.44
2	1.16	1.46	0.62	0.92	5.4	420	2.95	2.45
3	1.18	1.36	0.64	0.82	5.4	420	2.95	2.45
4	1.12	1.39	0.58	0.85	5.4	431	2.88	2.52
5	1.28	--[e]	0.74	--[e]	5.5	409	3.03	2.47
6	--[d]	--[d]	--[d]	--[d]	--[d]	410	3.02	--[d]
7	1.68	--[e]	1.14	--[e]	5.9	408	3.04	2.86
8	1.4	--[e]	0.86	--[e]	5.7	430	2.88	2.82
9	1.18	1.47	0.64	0.95	5.4	450	2.76	2.64

[(a)]Data collected versus decamethylferrocene/decamethyferrocenium (DMFc/DMFc$^+$) scale. [(b)]Data converted to the ferrocene/ferrocenium (Fc/Fc$^+$) scale: (DMFc/DMFc$^+$) was measured to be -0.54 vs. Fc/Fc$^+$ in DCM. [(c)]Estimated according to IP(s) = e$E_{1/2}^{+/0}$ [vs. Fc/Fc$^+$] + 4.8 eV. [(d)]Data could not be recorded, since compound **6** was not soluble in DCM. [(e)]Second oxidation state not detected in the potential window scanned.
[(f)]Value taken from onset of absorption in chloroform. Converted using E=1240/λ.

X-ray crystal structure analysis

The X-ray crystal structures of compounds **1**, **2**, **5**, **7** and **9** were obtained and the packing analyzed. The crystal structure of **9** was previously reported (CCDC287258).[36] Only compound **1** crystallizes in the orthorhombic *Pbca* space group, while all the other compounds crystallize in the same centrosymmetric space group No. 14, which is set as $P2_1/c$ for **2**, **4**, **9** and $P2_1/n$ for **5**, and **7** (Table 7). In all six crystals the reported molecules reside on inversion centers, thus only half a molecule is in the asymmetric unit and labeled. The substituents, which are the substituted phenyl rings in **1**, **2**, **4**, **5**, **7** and the thienyl rings in **9,** connected to C1 and C3 are in all cases not coplanar with the main pyrene core as is evident from Figure 10; the dihedral angles between the pyrene core and the phenyl rings (thienyl rings in **9**) are 53.9° and 57.3° for **1**, 44.4° and 67.2° for **2**, 41.7° and 53.0° for **4**, 44.8° and 44.8° for **5**, 53.6° and 53.8° for **7**, and 54.6° and 59.4° for **9.** The molecular structures of compound **9** as published before[36] and as synthesized in the course of the present

work hardly differ; for instance, the dihedral angles between the pyrene core and the thienyl rings in **9** are equal to 56.1° and 59.5° in Ref. 36 and the small differences in these parameters can be related to the difference in the temperatures of experiments. There are no short intermolecular contacts between molecules responsible for specific interactions such as π-π stacking interactions (see ESI).

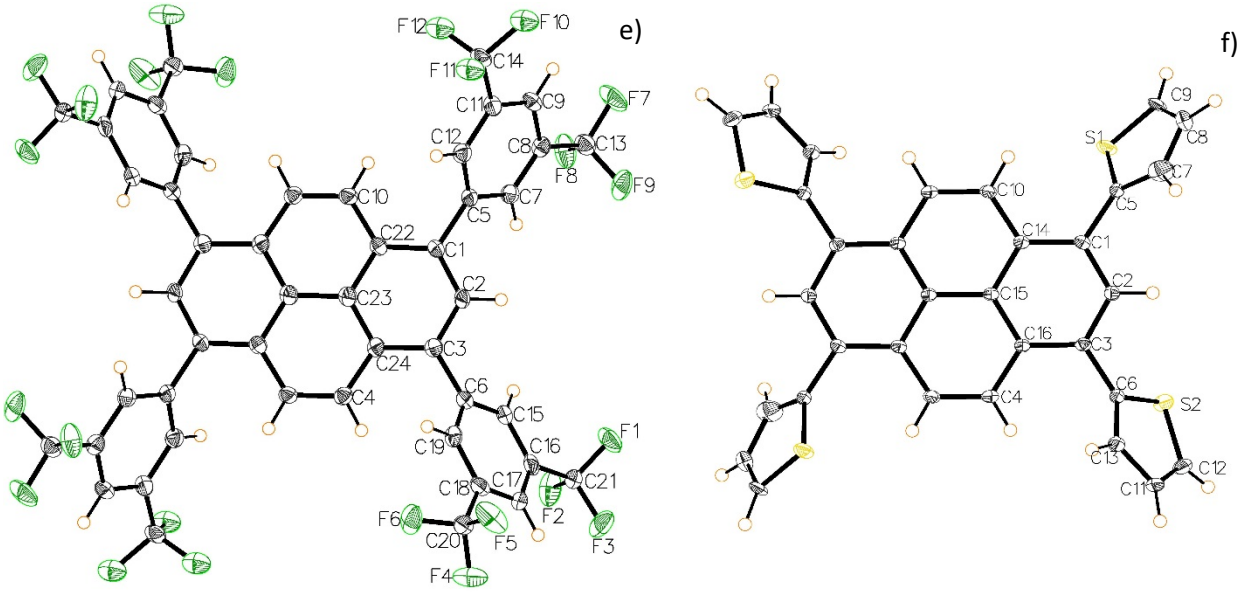

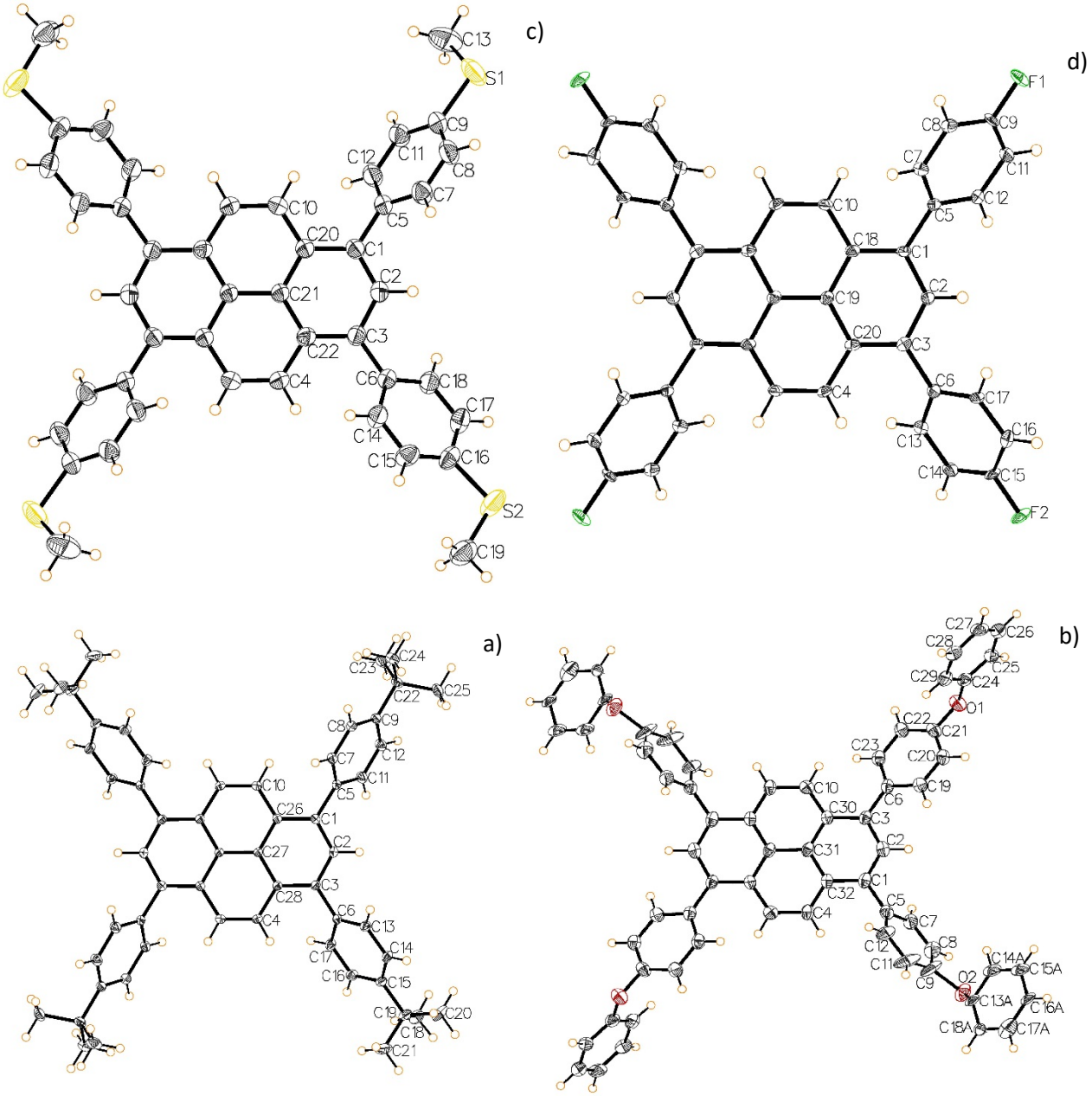

Figure 9. The molecular structures of compounds a) **1**, b) **2**, c) **4**, d) **5**, e) **7**, and f) **9**, showing the atomic numbering and 50% probability displacement ellipsoids.

Table 7. Main crystallographic data.

	1	**2**	**4**	**5**	**7**	**9**
Empirical formula	$C_{56}H_{58}$	$C_{64}H_{42}O_4$	$C_{44}H_{34}S_4$	$C_{40}H_{22}F_4$	$C_{48}H_{18}F_{24}$	$C_{32}H_{18}S_4$
Formula weight	731.02	875.04	690.95	578.61	1050.64	530.70
Temperature, K	100	100	297	100	100	100
Crystal system	orthorhombic	monoclinic	monoclinic	monoclinic	monoclinic	monoclinic
Space group	*Pbca*	*$P2_1/c$*	*P21/c*	*P21/n*	*P21/n*	*P21/c*
a, Å	14.829(6)	15.87(3)	16.4099(17)	3.914(3)	4.795(5)	13.688(3)
b, Å	12.324(5)	7.203(12)	6.9907(7)	11.932(10)	14.347(14)	8.4634(16)
c, Å	23.182(9)	19.66(3)	16.3466(17)	27.87(2)	28.88(3)	10.987(2)
α, °	90	90	90	90	90	90
β, °	90	106.884(17)	114.8800(10)	90.739(12)	92.154(14)	111.999(3)
γ, °	90	90	90	90	90	90
Volume, $Å^3$	4236(3)	2151(6)	1701.2(3)	1301.6(18)	1985(3)	1180.2(4)
Z	4	2	2	2	2	2
ρ_{calc}, g/cm^3	1.146	1.351	1.349	1.476	1.7576	1.493
F000	1576	916	724	596	1044	548
μ, mm^{-1}	0.064	0.083	0.312	0.104	0.181	0.425
Independent reflections	2913	1736	5209	2336	3678	5209
R_1; wR_2 ($I > 2\sigma(I)$)	0.0467, 0.0968	0.0552, 0.1115	0.0576, 0.1351	0.1071, 0.2833	0.0700, 0.1493	0.0335, 0.0891
GOF on F^2	1.050	1.090	1.018	1.064	1.029	1.060

OLED Device Data

Since **5**, **6**, **8** as well as **9** were characterized by low thin-film quantum yields, these compounds were considered less promising for application in OLEDs. Only compounds **2**, **3**, **4** as well as **7** were probed for their electroluminescent (EL) properties. Furthermore, the use of compound **1** in an OLED was reported in a patent application[60] and a recent publication.[61] Even though **7** is already patented, it was included in the device study because it is highly fluorinated and exhibits a high quantum yield in thin-film. The electroluminescent (EL) properties of compounds **2**, **3**, **4** and **7** were investigated in a standard ITO/PEDOT:PSS/[compounds]/Ca/Al sandwich geometry where the active layers were deposited by physical vapor deposition (PVD). Active layer thicknesses were 80 nm for all investigated devices. Figure 10a depicts the current density-voltage-luminescence (J-V-L) characteristics of devices with **2**, **3**, and **4** serving as the emissive layers. For the sake of better readability, the corresponding J-V-L characteristics of **7** are included in ESI. All relevant device parameters (turn-on voltage, maximum luminance, luminance efficiency) are listed in Table 8. Peak luminescence values of 85 cd m^{-2} at 6 V, 13542 cd m^{-2} at 8.2 V, and 6902 cd m^{-2} at 8 V were recorded for devices based on **4**, **2** and **3**, respectively. Low onset voltages of 2.9, 2.8, and 2.9 V were observed for **4**, **2**, and **3**, respectively; these values are close to the optical gap of approximately 2.6 eV of the investigated tetraryl pyrenes, which is indicative of efficient injection of charge carriers in all devices. Peak luminance efficiencies were 0.005 cd A^{-1} (4.6 V), 2 cd A^{-1} (3.6 V) and 2.6 cd A^{-1} (4.8 V) for **4**, **2** and **3**, respectively. These performance figures, with the exception of **4**, are rather impressive considering that these results were obtained from simple, not optimized single-layer geometries. Interestingly, devices based on **4** significantly trail the peak brightness and luminance efficiencies of the other two investigated tetraryl pyrenes, which is most likely explained by the presence of a charge carrier imbalance.

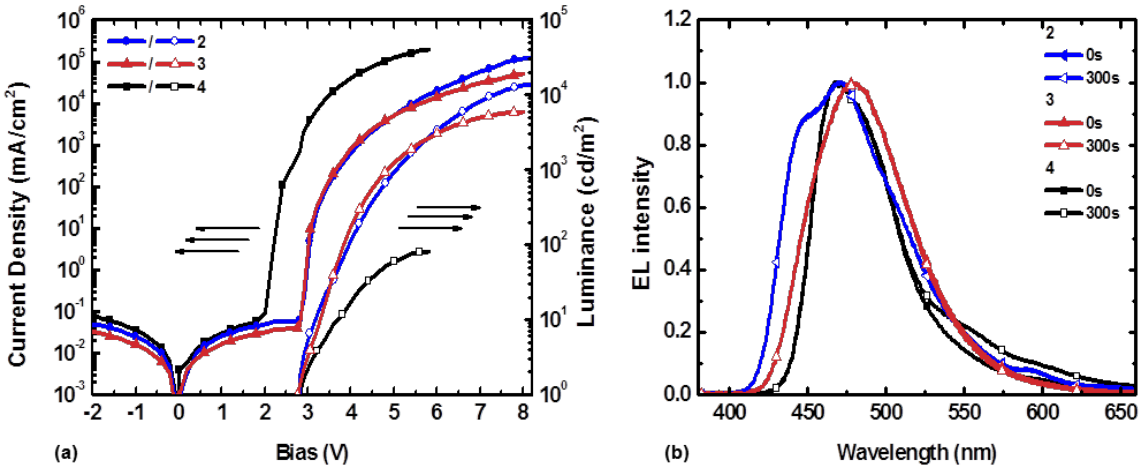

Figure 10. Current density (filed symbols) and luminance (open symbols) as a function of the bias voltage of ITO/PEDOT:PSS/**2**, **3**, **4**/Ca/Al devices (a) and the time-dependent evolution of the EL emission profile over the course of 5 minutes of continuous operation of **2**, **3** and **4** at an applied current density of 10^3 , $5x10^2$ and $4x10^4$ mA cm^{-2} respectively.

Interestingly, the trend of remarkably low onset voltages did not continue with the (trifluoromethyl)phenyl-decorated compound **7**, which turned-on at a rather high bias voltage of 9.0 V. Additionally, a peak luminance of **7** cd m^{-2} was attained at a quite high voltage of 12 V. Considering that **7** exhibited a PLQY close to unity in the thin-film, these findings indicate the presence of a severe charge carrier injection- and/or transport issue. While the CV data put the ionization potential of **7** at a deeper -5.9 eV compared to -5.4 eV of **2**, **3** and **4**, it is still noteworthy that the transition from the injection-limited conduction (ILC) - to the space-charge-limited current (SCLC)-regime is observable already at 3.9 V, which is less than half the onset voltage. Previous work on fluorinated fluorescent compounds by Lee et al.[62] also observed a significantly higher turn-on voltage for highly fluorinated compounds which they explained by the formation of transport-affecting charge traps by the electron-withdrawing fluorinated functionalities.[63] Additionally, it is possible that, similar to the observations made by Giebeler et al.[64], these bulk traps cause the buildup of an injection prohibiting counter field (similarly to the MEMOLED concept reported by Asadi et al.[65] where this field is generated by a ferroelectric).

EL properties and their time-evolution were observed over a period of 300 s of continuous operation and fixed current densities (see Figure 10b). Devices based on **4**, **2** and **3** featured sky-

blue emission color with a broad molecular emission peaking at 470, 471 and 479 nm, respectively, while **7** is characterized by a structure-less blue EL with a peak at 456 nm. Emission spectra of **3** were structure-less, the presence of a minor shoulder at 484 nm was detectable in the corresponding EL spectra of **4**. Regarding **2**, the appearance of a small emission peak at 593 nm, likely attributable to phosphorescent emission,[66-68] as well as the existence of a distinct shoulder at 450 nm are notable. From the thin-film PL spectra (see Figure 7) of **2** it is clear that the presence of microcavity effects[69] in the device led to an attenuation of the emission maximum at 450 nm and a boost of the small emission shoulder at 470 nm found in PL effectively exchanging the emission maximum and shoulder position in the corresponding EL spectra.

Owing to the additional high-energy contributions in the EL spectra of **7** and **2,** the Commission Internationale de l'Eclairage 1931 (CIE1931) (x, y) coordinates after power-on of **7** and **2** are (0.153, 0.124) and (0.163, 0.200), hence noticeably more blue than **4** and **3** based devices with (0.148, 0.244) and (0.148, 0,243). As can be inferred from the time evolution of the EL spectra depicted in Figure 10b no signs of material degradation are spectrally visible for **2** and **3** while hints of a degradation process are observable in the EL spectra of **4** by the formation of two shoulders at 555 nm and 593 nm after continuous operation of 300 s. Similarly, signs of material degradation were present in **7** where the emergence of a low energy emission with a small peak at 620 nm and the formation of distinct shoulders at 508 nm were evident. It is noted that all devices were free of any signs of excimer emission usually observable for unsubstituted pyrene.[70]

Overall, the presented tetraryl pyrenes already demonstrated impressive performance figures with respect to the obtained brightness and current efficiency values in non-optimized single-layer device architectures. Even more impressive were the observed turn-on voltages being as low as 2.8 V in a single-layer architecture, which are among the lowest for blue-emitting OLEDs.[71] In addition, the obtained performance values compare favorably to blue electrofluorescent devices with equally simple device architectures and active layers based on dendronized or polymerized pyrene derivatives.[72-75] Furthermore, by taking the human eye response curve into consideration, it has to be noted that the presented OLED devices are able to outperform the previously mentioned 1,3,6,8-tetrakis[4-2,2-diphenylvinyl)phenyl]pyrene multilayer devices based on the estimate that the human eye has $1/10^{th}$ the sensitivity at ~ 470 nm as at 545 nm. It is expected that device

efficiencies can be further improved by introduction of appropriate charge transport- and injection layers in order to ensure a more balanced charge injection and transport.[76]

Table 8. Electroluminescent characteristics of the investigated compounds in a single-layer geometry.

Compound	V_{on} [V][a)]	L_{max} [cd m^{-2}]	η [cd A^{-1}][b)]	CIE1931 [x y]
4	2.9	85	0.0050	0.148 0.244
2	2.8	13542	2.0000	0.163 0.200
7	8.6	7	0.0039	0.153 0.124
3	2.9	6902	2.6000	0.1480.243

[a)]voltage at a luminance of 1 cd m^{-2}; [b)]value of maximum efficiency

Conclusions

The series of nine 1,3,6,8-tetraarylpyrenes exhibit positive solvatochomic behavior. DFT calculations verify the $S_0 \rightarrow S_1$ transition to be HOMO-LUMO character as observed for 1,3,6,8-tetraphenylpyrene and in contrast to pyrene. The fluorescence quantum yield in solution ranged from 0.76 (**6**) to 0.98 (**2**), while the quantum yield peaked for compound **7** in the solid state at 0.91. The absence of short-contacts and interactions in the solid state was verified by X-ray crystallography. Compounds **2**, **3**, **4**, and **7** were tested in OLED in an unoptimized single-layer device geometry and exhibited blue electroluminescence with low turn-on voltages and high maximum luminances. An efficient injection of charge carriers was observed for all devices.

Acknowledgments

This work was supported the University Research Board of the American University of Beirut. The authors are grateful for this support. B.R.K. and B.W. acknowledge the Arab Fund Scholarship Program for financial support. The authors thank Dr. Veaceslav Coropceanu, Mr. Alexandr Fonari and Mr. Stephen B. Shirring for fruitful discussions. M.A. gratefully acknowledges the financial support of the Klima- und Energiefonds Project PLASMOLED 3726090.

References

1. Y. Chen, Q. Lv, Z. Q. Liu and Q. Fang, *Inorg. Chem. Commun.*, 2015, **52**, 38-40.
2. A. Singh, R. Singh, M. Shellaiah, E. C. Prakash, H. C. Chang, P. Raghunath, M. C. Lin and H. C. Lin, *Sensor Actuat. B-Chem.*, 2015, **207**, 338-345.
3. R. W. Sinkeldam, N. J. Greco and Y. Tor, *Chem. Rev.*, 2010, **110**, 2579-2619.
4. T. M. Figueira-Duarte and K. Müllen, *Chem. Rev.*, 2011, **111**, 7260-7314.
5. V. Balzani, P. Ceroni and A. Juris, *Photochemistry and Photophysics: Concepts, Research, Applications*, Wiley, 2014.
6. B. Valeur and M. N. Berberan-Santos, *Molecular Fluorescence: Principles and Applications*, John Wiley & Sons, 2013.
7. J. B. Birks, *Photophysics of Aromatic Molecules*, 1970.
8. I. B. Berlman, *Handbook of Fluorescence Spectra of Aromatic Molecules*, Academic Press, New York, 1971.
9. C. A. Parker and C. G. Hatchard, *Trans. Faraday Soc.*, 1963, **59**, 284-&.
10. G. K. Bains, S. H. Kim, E. J. Sorin and V. Narayanaswami, *Biochemistry*, 2012, **51**, 6207-6219.
11. M. Shimizu and T. Hiyama, *Chem. - Asian J.*, 2010, **5**, 1516-1531.
12. J. M. Casas-Solvas, J. D. Howgego and A. P. Davis, *Org. Biomol. Chem.*, 2014, **12**, 212-232.
13. H. Maeda, T. Maeda, K. Mizuno, K. Fujimoto, H. Shimizu and M. Inouye, *Chem. - Eur. J.*, 2006, **12**, 824-831.
14. C.-H. Yang, T.-F. Guo and I. W. Sun, *J. Lumin.*, 2007, **124**, 93-98.
15. T. M. Figueira-Duarte, S. C. Simon, M. Wagner, S. I. Druzhinin, K. A. Zachariasse and K. Müllen, *Angew. Chem., Int. Ed.*, 2008, **47**, 10175-10178.
16. J. A. Mikroyannidis, *Synth. Met.*, 2005, **155**, 125-129.
17. J. Grimshaw and J. Trocha-Grimshaw, *J. Chem. Soc., Perkin Trans. 1*, 1972, 1622-1623.
18. A. a. O. El-Ballouli, R. S. Khnayzer, J. C. Khalife, A. Fonari, K. M. Hallal, T. V. Timofeeva, D. Patra, F. N. Castellano, B. Wex and B. R. Kaafarani, *J. Photochem. Photobiol., A*, 2013, **272**, 49-57.
19. A. G. Crawford, A. D. Dwyer, Z. Liu, A. Steffen, A. Beeby, L.-O. Palsson, D. J. Tozer and T. B. Marder, *J. Am. Chem. Soc.*, 2011, **133**, 13349-13362.
20. B. R. Kaafarani, A. a. O. El-Ballouli, R. Trattnig, A. Fonari, S. Sax, B. Wex, C. Risko, R. S. Khnayzer, S. Barlow, D. Patra, T. V. Timofeeva, E. J. W. List, J.-L. Bredas and S. R. Marder, *J. Mater. Chem. C*, 2013, **1**, 1638-1650.
21. X. Feng, J.-Y. Hu, L. Yi, N. Seto, Z. Tao, C. Redshaw, M. R. J. Elsegood and T. Yamato, *Chem. - Asian J.*, 2012, **7**, 2854-2863.
22. X. Feng, J.-Y. Hu, F. Iwanaga, N. Seto, C. Redshaw, M. R. J. Elsegood and T. Yamato, *Org. Lett.*, 2013, **15**, 1318-1321.
23. T. Makowski, R. M. Moustafa, P. Uznanski, W. Zajaczkowski, W. Pisula, A. Tracz and B. R. Kaafarani, *J. Phys. Chem. C*, 2014, **118**, 18736-18745.
24. S. Chen, F. S. Raad, M. Ahmida, B. R. Kaafarani and S. H. Eichhorn, *Org. Lett.*, 2013, **15**, 558-561.
25. J. N. Moorthy, P. Natarajan, P. Venkatakrishnan, D.-F. Huang and T. J. Chow, *Org. Lett.*, 2007, **9**, 5215-5218.
26. J.-Y. Hu, X. Feng, H. Tomiyasu, N. Seto, U. Rayhan, M. R. J. Elsegood, C. Redshaw and T. Yamato, *J. Mol. Struct.*, 2013, **1047**, 194-203.
27. P. Anant, N. T. Lucas, J. M. Ball, T. D. Anthopoulos and J. Jacob, *Synth. Met.*, 2010, **160**, 1987-1993.
28. T. Oyamada, H. Uchiuzou, S. Akiyama, Y. Oku, N. Shimoji, K. Matsushige, H. Sasabe and C. Adachi, *J. Appl. Phys.*, 2005, **98**, 074506/074501 - 074506/074507.
29. Z.-Q. Liang, Z.-Z. Chu, D.-C. Zou, X.-M. Wang and X.-T. Tao, *Org. Electron.*, 2012, **13**, 2898-2904.

30. K. C. Stylianou, R. Heck, S. Y. Chong, J. Bacsa, J. T. A. Jones, Y. Z. Khimyak, D. Bradshaw and M. J. Rosseinsky, *J. Am. Chem. Soc.*, 2010, **132**, 4119-4130.
31. D. R. Coulson, *Inorg. Synth.*, 1990, **28**, 107-109.
32. G. Huang, Y.-Q. Sun, Z. Xu, M. Zeller and A. D. Hunter, *Dalton Trans.*, 2009, 5083-5093.
33. V. de Halleux, J. P. Calbert, P. Brocorens, J. Cornil, J. P. Declercq, J. L. Bredas and Y. Geerts, *Adv. Funct. Mater.*, 2004, **14**, 649-659.
34. C. S. Callam and T. L. Lowary, *J. Chem. Educ.*, 2001, **78**, 947-948.
35. Y. Sagara, T. Mutai, I. Yoshikawa and K. Araki, *J. Am. Chem. Soc.*, 2007, **129**, 1520-1521.
36. H. J. Zhang, Y. Wang, K. Z. Shao, Y. Q. Liu, S. Y. Chen, W. F. Qiu, X. B. Sun, T. Qi, Y. Q. Ma, G. Yu, Z. M. Su and D. B. Zhu, *Chem. Commun.*, 2006, 755-757.
37. T. Korzdörfer, J. S. Sears, C. Sutton and J. L. Brédas, *J. Chem. Phys.*, 2011, **135**, 204107.
38. S. Refaely-Abramson, R. Baer and L. Kronik, *Phys. Rev. B*, 2011, **84**.
39. Gaussian 09, Revision D.01, M. J. Frisch, G. W. Trucks, H. B. Schlegel, G. E. Scuseria, M. A. Robb, J. R. Cheeseman, G. Scalmani, V. Barone, B. Mennucci, G. A. Petersson, H. Nakatsuji, M. Caricato, X. Li, H. P. Hratchian, A. F. Izmaylov, J. Bloino, G. Zheng, J. L. Sonnenberg, M. Hada, M. Ehara, K. Toyota, R. Fukuda, J. Hasegawa, M. Ishida, T. Nakajima, Y. Honda, O. Kitao, H. Nakai, T. Vreven, J. A. Montgomery, Jr., J. E. Peralta, F. Ogliaro, M. Bearpark, J. J. Heyd, E. Brothers, K. N. Kudin, V. N. Staroverov, R. Kobayashi, J. Normand, K. Raghavachari, A. Rendell, J. C. Burant, S. S. Iyengar, J. Tomasi, M. Cossi, N. Rega, J. M. Millam, M. Klene, J. E. Knox, J. B. Cross, V. Bakken, C. Adamo, J. Jaramillo, R. Gomperts, R. E. Stratmann, O. Yazyev, A. J. Austin, R. Cammi, C. Pomelli, J. W. Ochterski, R. L. Martin, K. Morokuma, V. G. Zakrzewski, G. A. Voth, P. Salvador, J. J. Dannenberg, S. Dapprich, A. D. Daniels, Ö. Farkas, J. B. Foresman, J. V. Ortiz, J. Cioslowski, and D. J. Fox, Gaussian, Inc., Wallingford CT, 2009.
40. R. J. Lakowicz, *Principles of Fluorescence Spectroscopy*, Plenum Press, New York, 1983.
41. SAINTPlus., Bruker AXS, Madison, WI, v. 6.2 edn., 2001.
42. G. M. Sheldrick, Bruker AXS, Madison, WI, V.2.0.3, Bruker/Siemens area detector absorption correction program edn., 2003.
43. O. V. Dolomanov, L. J. Bourhis, R. J. Gildea, J. A. K. Howard and H. Puschmann, J*. Appl. Cryst.,* 2009, 4**2,** 339-341.
44. M. Sase, S. Yamaguchi, Y. Sagara, I. Yoshikawa, T. Mutai and K. Araki, J*. Mater. Chem.,* 2011, 2**1,** 8347-8354.
45. M. Parac and S. Grimme, C*hem. Phys.,* 2003, 2**92,** 11-21.
46. Across various reports in literature, the numbering of pyrene is inconsistent. Herein we strictly follow the numbering of pyrene according to IUPAC nomenclature.
47. O. K. Bazyl, G. V. Maier, T. N. Kopylova and V. I. Danilova, Z*.Prik. Spekt.,* 1982, 3**7,** 80-86.
48. WO2006057326A1, 2006.
49. N. Nijegorodov, V. Zvolinsky and P. V. C. Luhanga, J*. Photochem. Photobiol., A,* 2008, 1**96,** 219-226.
50. K. R. Idzik, T. Licha, V. Lukes, P. Rapta, J. Frydel, M. Schaffer, E. Taeuscher, R. Beckert and L. Dunsch, J*. Fluoresc.,* 2014, 2**4,** 153-160.
51. J. T. Henssler, X. N. Zhang and A. J. Matzger, J*. Org. Chem.,* 2009, 7**4,** 9112-9119.
52. N. Mataga and T. Kubota, M*olecular Interactions of Electronic Spectra,* Marcel Kekker, New York, 1970.
53. Q. Feng, M. Wang, B. Dong, C. Xu, J. Zhao and H. Zhang, C*ryst. Eng. Comm.,* 2013, 1**5,** 3623-3629.
54. A. T. Haedler, H. Misslitz, C. Buehlmeyer, R. Q. Albuquerque, A. Köhler and H.-W. Schmidt, C*hemPhysChem,* 2013, 1**4,** 1818-1829.
55. S. M. Ryno, C. Risko and J. L. Bredas, J*. Am. Chem. Soc.,* 2014, 1**36,** 6421-6427.

56. T. Oyamada, S. Akiyama, M. Yahiro, M. Saigou, M. Shiro, H. Sasabe and C. Adachi, C*hem. Phys. Lett.,* 2006, 4**21,** 295-299.
57. M. Gingras, V. Placide, J. M. Raimundo, G. Bergamini, P. Ceroni and V. Balzani, C*hem. - Eur. J.,* 2008, 1**4,** 10357-10363.
58. J. Phelps, K. S. V. Santhanam and A. J. Bard, J*. Am. Chem. Soc.,* 1967, 8**9,** 1752-1753.
59. L. S. Marcoux, J. M. Fritsch and R. N. Adams, J*. Am. Chem. Soc.,* 1967, 8**9,** 5766-5769.
60. US Pat., US20100164374A1, 2010.
61. W. Sotoyama, H. Sato, M. Kinoshita, T. Takahashi, A. Matsuura, J. Kodama, N. Sawatari and H. Inoue, D*ig. Tech. Pap. - Soc. Inf. Disp. Int. Symp.,* 2003, 3**4,** 1294-1297.
62. J. K. Lee, H. H. Fong, A. A. Zakhidov, G. E. McCluskey, P. G. Taylor, M. Santiago-Berrios, H. D. Abruna, A. B. Holmes, G. G. Malliaras and C. K. Ober, M*acromolecules,* 2010, 4**3,** 1195-1198.
63. L. J. Alvey, R. Meier, T. Soos, P. Bernatis and J. A. Gladysz, E*ur. J. Inorg. Chem.,* 2000, 2**000,** 1975-1983.
64. C. Giebeler, S. A. Whitelegg, A. J. Campbell, M. Liess, S. J. Martin, P. A. Lane, D. D. C. Bradley, G. Webster and P. L. Burn, A*ppl. Phys. Lett.,* 1999, 7**4,** 3714-3716.
65. K. Asadi, P. W. M. Blom and D. M. de Leeuw, A*dv. Mater.,* 2011, 2**3,** 865-868.
66. J. M. Lupton, A. Pogantsch, T. Piok, E. J. W. List, S. Patil and U. Scherf, P*hys. Rev. Lett.,* 2002, 8**9.**
67. L. Qian, D. Bera and P. H. Holloway, A*ppl. Phys. Lett.,* 2007, 9**0,** 153120-153123.
68. M. A. Omary, R. M. Kassab, M. R. Haneline, O. Elbjeirami and F. P. Gabbai, I*norg. Chem.,* 2003, 4**2,** 2176-2178.
69. V. Bulovic, V. B. Khalfin, G. Gu, P. E. Burrows, D. Z. Garbuzov and S. R. Forrest, P*hys. Rev. B,* 1998, 5**8,** 3730-3740.
70. S. M. Langenegger and R. Haner, C*hem. Commun.,* 2004, 2792-2793.
71. P. Kotchapradist, N. Prachumrak, R. Tarsang, S. Jungsuttiwong, T. Keawin, T. Sudyoadsuk and V. Promarak, J*. Mater. Chem. C,* 2013, 1**,** 4916-4924.
72. T. M. Figueira-Duarte, P. G. Del Rosso, R. Trattnig, S. Sax, E. J. W. List and K. Müllen, A*dv. Mater.,* 2010, 2**2,** 990-993.
73. T. S. Qin, W. Wiedemair, S. Nau, R. Trattnig, S. Sax, S. Winkler, A. Vollmer, N. Koch, M. Baumgarten, E. J. W. List and K. Mullen, J*. Am. Chem. Soc.,* 2011, 1**33,** 1301-1303.
74. C. J. Ou, Z. F. Lei, M. L. Sun, L. H. Xie, Y. Qian, X. W. Zhang and W. Huang, S*ynth. Met.,* 2015, 2**00,** 135-142.
75. G. Zhang, M. Baumgarten, M. Auer, R. Trattnig, E. J. W. List-Kratochvil and K. Müllen, M*acromol. Rapid Commun.,* 2014, 3**5,** 1931-1936.
76. R. Trattnig, L. Pevzner, M. Jager, R. Schlesinger, M. V. Nardi, G. Ligorio, C. Christodoulou, N. Koch, M. Baumgarten, K. Müllen and E. J. W. List, A*dv. Funct. Mater.,* 2013, 2**3,** 4897-4905.